Revista GEOCIÊNCIAS

unesp

ISSN: 1980-900X (online)

PETROPHYSICAL CHARACTERIZATION OF THE PALAEOZOIC AMOTAPE GROUP IN THE COLÁN BLOCK: A POTENTIAL UNCONVENTIONAL HYDROCARBON TARGET IN THE TALARA BASIN (NW PERU)

CARACTERIZAÇÃO PETROFÍSICA DO GRUPO AMOTAPE PALEOZOICO NO BLOCO COLÁN: UM POTENCIAL ALVO NÃO-CONVENCIONAL PARA HIDROCARBONETOS NA BACIA TALARA (NW DO PERU)

Jul Roldán GUEVARA[1,2], Eduardo A. ROSSELLO[3,4], Sergio A. LÓPEZ ISAZA[4], Carlos MARISCAL[1].

[1]Universidad Nacional de San Antonio Abad del Cusco (UNSAAC).
[2]Zeus Energy SAC, Peru. Dirección: Av. Sánchez Cerro No. 234 – Zona - Edificio Real Plaza – Oficina O-701, Piura, Peru. Email: julroldang@gmail.com
[3]Universidad de Buenos Aires. Instituto de Geociencias Básicas (IGEBA-CONICET). Departamento de Ciencias Geológicas. Pabellón II, Ciudad Universitaria, 1428 – Buenos Aires, Argentina. Email: ea_rossello@yahoo.com.ar
[4]Departamento de Ciencias Geológicas, Universidad de Buenos Aires, Pabellón II, Ciudad Universitaria, 1428 Buenos Aires, Argentina. Email: seadlois@gmail.com

ABSTRACT - The Amotape Group consists of metasedimentites with varying degrees of metamorphism and Paleozoic intrusions, exposed as isolated blocks that form an NNE-SSW belt, separating the Meso-Cenozoic depocenters of the Talara (west) and Sechura and Tumbes basins (east) along the Pacific margin of NW Peru. We describe three metamorphic/tectonic episodes that produced sub-planar structures (cleavages, fractures) affecting the rocks of the Amotape Group, allowing this unit to be classified as a fractured reservoir. Field survey and multi-scale subsurface data from the Colán Block, evidence a secondary porosity system associated with fracture networks that affect both the basin fill and the basement units. This configures a complementary unconventional exploration target. Sandstone levels in lateral contact with leptometamorphic rocks of the Amotape Group define good reservoir potential due to the preferentially brittle mechanical behavior of the basement, which develops abundant fractures. The porosity values of the Amotape Group range between 4.62% and 1.23%, while permeabilities are on the order of 0.519-0.016 mD. Elevated trapping positions seem to be successfully sealed by Cretaceous units. The reservoir properties define a complementary play concept that could be extended to other positions of the technical basement in the Talara Basin and analogous regions.

Keywords: Amotape Group. Paleozoic. Unconventional reservoir. Hydrocarbon potential. Talara Basin. Fracture porosity.

RESUMO - O Grupo Amotape é composto por metassedimentitos com graus variados de metamorfismo e intrusões paleozoicas, expostos como blocos isolados que formam um cinturão NNE-SSW, separando os depocentros meso-cenozoicos das bacias Talara (oeste) e Sechura e Tumbes (leste) ao longo da margem pacífica do noroeste do Peru. São descritos três episódios metamórficos/tectônicos que produziram estruturas subplanares (clivagens, fraturas) afetando as rochas do Grupo Amotape, permitindo que esta unidade seja classificada como um reservatório fraturado. Levantamentos de campo e dados de subsuperfície em múltiplas escalas do Bloco Colán evidenciam um sistema de porosidade secundária associado a redes de fraturas que afetam tanto o preenchimento da bacia quanto as unidades do embasamento. Isto configura um alvo complementar de exploração não convencional. Níveis de arenito em contato lateral com rochas anquimetamórficas do Grupo Amotape definem bom potencial de reservatório devido ao comportamento mecânico preferencialmente frágil do embasamento, que desenvolve fraturas abundantes. Os valores de porosidade do Grupo Amotape variam entre 4,62% e 1,23%, enquanto as permeabilidades são da ordem de 0,519-0,016 mD. As posições de trapas elevadas parecem ter sido seladas com sucesso pelas unidades do Cretáceo. As propriedades do reservatório definem um conceito de play complementar que poderia ser estendido a outras posições do embasamento técnico na Bacia de Talara e regiões análogas.

Palavras-chave: Grupo Amotape. Paleozoico. Reservatório não convencional. Potencial para hidrocarbonetos. Bacia Talara. Porosidade por fraturas.

INTRODUCTION

The Talara Basin encompasses 15,000 km^2 of the northwestern Pacific margin of Perú (Figure 1), where the oceanic Nazca Plate is being subducted beneath the continental South American Plate (Travis et al., 1976; Cobbold et al., 2007; Diniz et al., 2010; Espurt et al., 2018; Lemgruber-Traby et al., 2020). Palaeozoic basement is being exposed intermittently in the La Brea, Amotape, Silla de Paita and Illescas mountains, which extend along 250 km trending 60º towards the NE (Palacios, 1994; Palacios et al., 2004).

The Amotape Gr is made up of lithologies with different degrees of metamorphism and other Palaeozoic intrusive rocks that sporadically crop out along an NNE-SSE corridor on the Pacific margin of Perú and it separates the Talara (west), Sechura, Lancones and Tumbes (east) basins (Figure 1). The southern boundary of the Talara basin is the La Silla de Paita (Aizprua et al., 2019). Higley (2004) mentioned that the hydrocarbon production of the Talara Basin achieved 1.68 billion barrels of oil during the last ~ 130 years, being recovered from the traditional Cretaceous and Paleogene-Neogene reservoirs.

Daily production from the Eocene sandstone reservoirs located onshore is of around 15,000 BOE recovered from more than 2,600 active wells in an area of 460 km². The remaining recoverable volume could reach 120 MMBOE (Perupetro, 2020). Wells depth range between 500 and 2,800 m, and the quality of oil is remarkably good, with average gravity of 33° API (25°- 42° range) and very low sulphur content (Hinoztrosa & Espinoza, 2005).

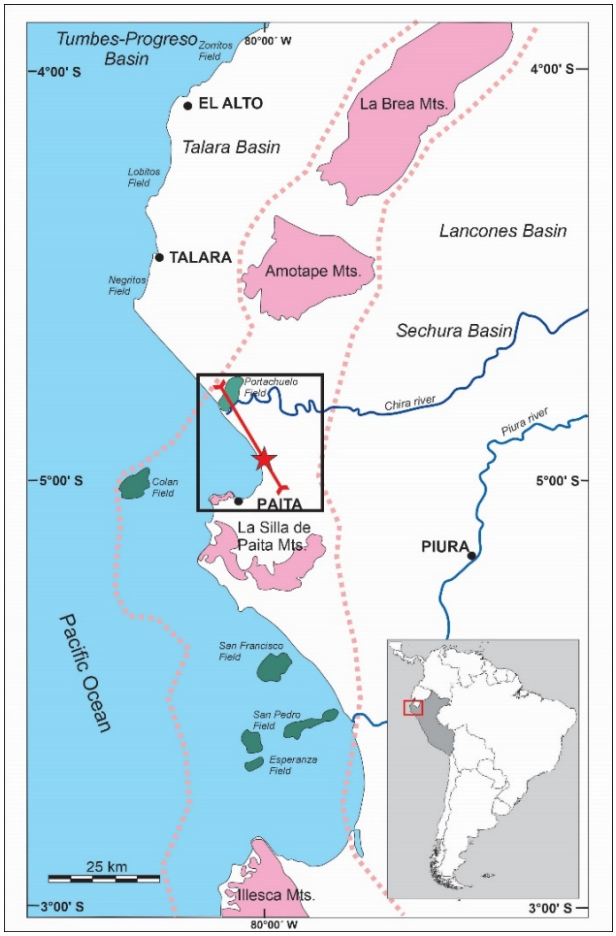

Figure 1 - Location of the study area on the NW coast of Peru showing the outcrops of the Amotape Group in pink areas (taken from Valencia and Llerena, 2018) following an NNE-SSW corridor that separates the Meso-Cenozoic depocenters of the Talara, Tumbes-Progreso and Sechura basins. In green are off-shore field on Amotape Group. The insert black square highlights the location of the Colán well (red star) and the seismic line of Figure 11.

The interest in hydrocarbon exploration on the Palaeozoic Amotape Group had its beginnings by the mid-1940s (Nauss, 1944; Newell et al., 1949). Several works have described main petrographic hydrocarbon characteristics of those rocks making this unit a potential target into the petroleum system with commercial production in the Talara Basin (Martínez, 1970; Palacios,

1994; Fildani et al., 2005, 2008; Bellido et al., 2008; Portella-Villachica, 2018).

The first production of the Palaeozoic Amotape Group corresponds to the hydrocarbon discovery by wildcat No. 4610 in 1954, located in the northeast edge of the Portachuelo high (Prado-Paucar, 2018). Rocks of the Amotape Group in the basement of the producing fields in the Talara, Sechura and Tumbes basins are mainly made up of magmatic and metamorphic rocks with recognized (or expected) good conditions for unconventional fractured reservoirs (Perupetro, 1970; Pindell & Tabbot, 1995). In the case of the Talara Basin, the Palaeozoic basement rocks hold attractive geological characteristics that represent a challenge to define its potential as a commercial reservoir due to their complex fracture network and lithological heterogeneity.

We have petrophysically characterised the rocks of the Amotape Group using surface information (strategic outcrops, mapping, etc.), subsurface data (2D seismic, well logs) and petrographic studies of rocks outcropping in the Colán area of NW Peru. The results of this multi-scale approach could be extrapolated to other geological regions of the Talara basin and other prospective areas of NW Peru, including the mature fields of Portachuelo, Laguna and San Pedro fields (Figure 2) where it is assumed that the frontier play of fractured basement could be actively working.

GEOLOGICAL FRAMEWORK

The study region comprises the southern portion of the metamorphic belt of the Amotape Mountains, which is composed of thick units of slates, schists, and quartzites cropping out in the neighbouring Cerro La Brea as well as the surroundings of Paita city (Figure 1). The stratigraphic infill of the Talara Basin consists of predominantly siliciclastic facies, comprising Mesozoic, late Eocene, and Quaternary ages (Figure 2). These units have been studied from onshore and offshore subsurface information and outcrop (surface) data, where they are covered in ~90% by the Pliocene-Quaternary marine terraces of the Tablazo Formation (Valencia and Llerena, 2018).

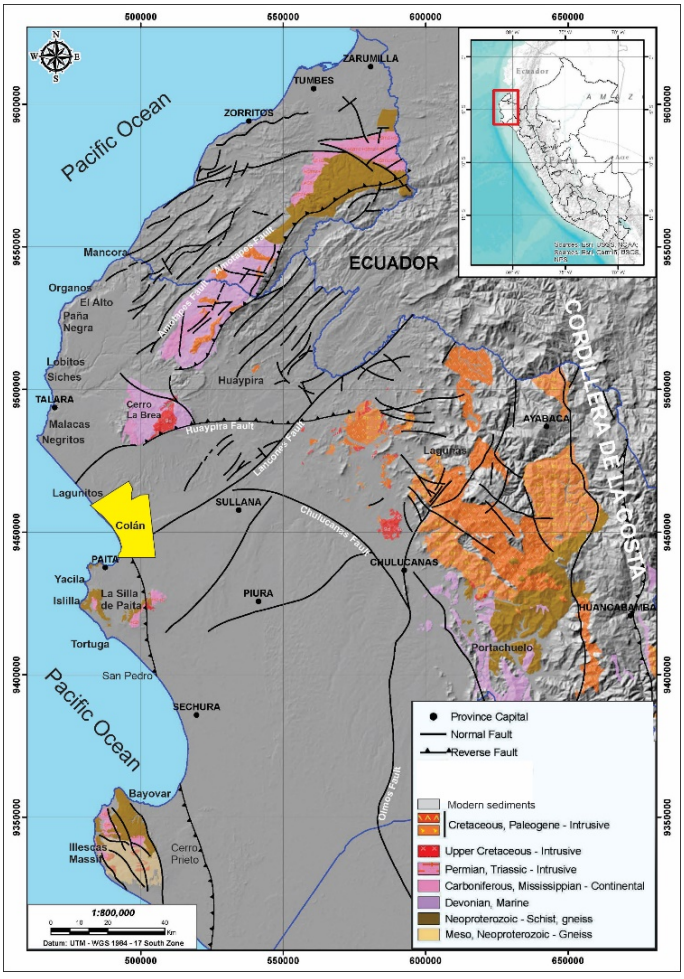

Figure 2. Geological map with the distribution of the main igneous and metamorphic Palaeozoic basement rocks, comprising predominantly siliciclastic facies Mesozoic, late Eocene, and Quaternary ages (taken from Bellido et al., 2009). Yellow polygon is the Colan Block.

Stratigraphic record

The complete stratigraphic record of the Talara Basin consists of the following three regionally distributed geological units:

i) *the Palaeozoic unit*, with about 2,400 m composed of metamorphic rocks and associated igneous intrusions, it constitutes the technical basement of the entire Cretaceous-Cenozoic Talara Basin,

ii) *the Cretaceous sequence*, made up of about 2,700 m of platform carbonate levels and shales deposited in restricted marine environments, with some sandstone intercalations, and

iii) *the Cenozoic infill*, formed by about 5,000 m of layers of sedimentary rocks deposited in fluvio-deltaic, tidal, shallow-marine, and deep-marine turbiditic environments, in a retro-arc position during normal ocean-continent subduction (Fildani et al., 2005, 2008).

Palaeozoic

The name "Amotape Group" was derived from the Amotape Mountains distributed between the Peruvian and Ecuadorian territories with a general orientation NNE-SSW (Iddings & Olsson, 1928). The Palaeozoic rocks of the Amotape Group, initially described by Bosworth (1923), are the oldest rocks in the region (Figure 3). The southernmost outcrop in Illescas is also considered by Bianchi & Jacay (2015) to include Precambrian metamorphic series forming part of the Cordillera de la Costa (Figure 2). Cardona et al. (2009) indicated zircon U-Pb ages of 280 to 1,690 Ma for the crystalline rocks, orthogneisses, and migmatites in the core of the Illescas outcrops. However, this author considered the upper part of the unit as lower Palaeozoic, that exhibits less intense metamorphism and deformation.

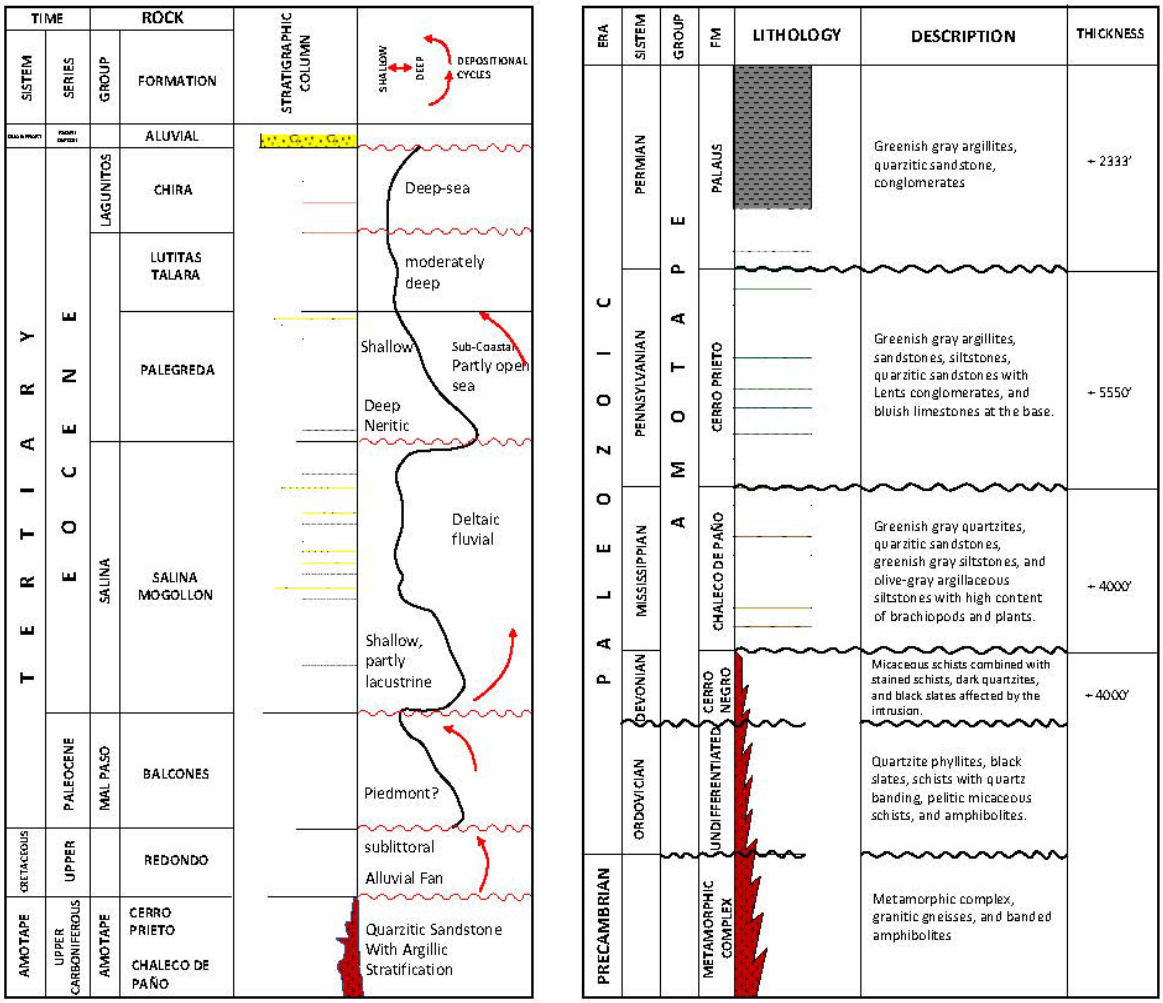

Figure 3. ***Left***: Stratigraphic chart of the Talara Basin (from Grover Gonzales, 1967). ***Right***: Paleozoic and Precambrian stratigraphic column of the Talara Basin (taken from Valencia and Llerena, 2018 in Palacios, 1994).

In the southern part of the Amotape mountains the older outcrops are unconformably overlain by the Devonian Cerro Negro Formation, the Mississippian Chaleco de Paño Formation, the Pennsylvanian Cerro Prieto Formation, and the Permian Palaus Formation. These units probably correspond to the oldest rocks exposed in NW Peru being affected by regional metamorphism.

They form a series of uplifted blocks along the eastern sides of both the Tumbes and Talara basins as well as the basement of the latter (Fildani et al., 2008). Palacios (1994) described the Metamorphic Series of Paita cropping out in the surroundings of the homonymous town, attributing them an Ordovician-Silurian age, and being constituted by dark grey micaceous slates and schists, and folded quartzites with thin bedding and intraformational faulting.

The Amotape Group consists of deformed low-grade metamorphic rocks with Devonian to Permian ages (Shepherd & Moberly, 1981) represented by typical fauna remains that include the goniatite species *Pseudoparalogoceras peruviana*, and fusulinids indicating a middle Pennsylvanian (Atokan) age. This unit consists of monotonous, rhythmic, and deformed sequences of sandstone, quartzite, claystone, and black slate, locally deposited in a littoral environment, and intruded by granites. In the Andean foreland, marine strata of the Amotape Group are correlated with facies of the Tarma-Copacabana Group (Newell et al., 1949).

The intrusive rocks in the basal part of the Amotape Group are composed by grey tonalitic orthogneisses with bands of quartz-feldspar and biotite-muscovite-amphiboles (Caldas et al., 1979). In the core of the succession appear migmatites grading to anatectic granites and tonalites of probable Upper Triassic age, associated to micaceous schists interbedded with quartzite in thin layers, showing ductile deformation (Cardona et al., 2009; Bellido et al., 2009). Towards the upper part there is an intercalation of schists, phyllites, slates and quartzites evidencing a lesser degree of regional metamorphism. The La Silla de Paita hill (Figure 2) is made up of a gneissified granitic body that intrudes metamorphic rocks, and in the Amotape - La Brea massifs these intrusions are linked to felsic bodies (Palacios, 1994). In the Paita-Islilla area, orthogneiss occurs intruding sequences of schists, slates, and quartzites, indicating great similarity to what was reported in Tumbes Basin and its northern projection into Ecuador (Caldas, 1979; Cardona et al., 2009).

Martínez (1970) described a total stratigraphic thickness of approximately 5,000 m for the Amotape Group, which can be subdivided into the following four formations: Cerro Negro, Chaleco de Paño, Cerro Prieto, and Palaus (Figure 3):

a) The Cerro Negro Formation crops out in the Illescas hills and represents 1,300 m of metamorphosed siliciclastic sediments, composed of micaceous schists, dark quartzites and carbonaceous slates with anisotropies predominantly striking NE-SW.

b) The Chaleco de Paño Formation crops out in ravines, and forms a predominantly NE-trending, 1,300 m-thick succession consisting of dark quartzites and grey to greenish phyllites.

c) The Cerro Prieto Formation is made up of Carboniferous rocks outcrop out as 1,800 m-thick succession that consists of dark grey to black shale with brachiopod-bearing marine sandstones (Figure 2). Martínez (1970) describes up to 27 bodies of quartzite sandstones to concretionary and brecciated mudstones and metapelites, with some fractured limestone horizons. In general, these rocks have undergone very incipient metamorphism, which could be considered more like advanced diagenesis. The predominant NE-EW anisotropies are deflecting to NW-SE and dipping from low angles to vertical (Cerro Prieto).

d) The Palaus Formation crops out in the western part of the Amotape Mountains. This youngest portion of the Palaeozoic basement is attributed to the Permian. It consists of an 800 m-thick basal sequence of impure and lenticular limestones, followed by sandstones, mudstones, and lenticular conglomerates, with a predominance of grey shales towards the top. The degree of metamorphism is very incipient (advanced diagenesis only) to non-existent. In total, 8 sandstone bodies with variable thicknesses between 7,5 and 25 m are observed. Strata predominantly strike N-S to NW.

Bellido et al. (2009) described two assemblages of S-type granites in the Amotape Group, composed of: **i**) peraluminous migmatite granites and migmatites in an autochthonous catazonal domain (Illescas Massif), and **ii**) biotitic monzo-granites with cordierite and leucogranites, emplaced in siliciclastic epizonal metasediments providing a U-Pb age of 220 ± 1.5 Ma and a metamorphic peak age of 239 ± 2 Ma in residual material. Both units were derived from metasediment melting and are likely to be geneti-cally related, and anatexis was apparently devel-oped in relation with extensional deformation. The crustal thickening of the margin in the Palaeozoic, followed by the rifting phase that started during the mid-Triassic, explains this granitic association prior to the subsequent separation, transcurrent migration, accretion, and deformation of the para-autochthonous Amotape Group terrane by the Jurassic (Fildani et al., 2008; Nocquet et al., 2014).

Cretaceous to Eocene succession

These sequences consist of siliciclastic rocks of multiple origins and total thickness in excess of 9,000 m. However, outcrops are not well exposed in any part of the basin and the few known ones on the coast are difficult to access (Jaillard, 1990). Carozzi & Palomino (1993) and Fildani et al. (2008) describe a gradual deepening trend towards the west into a deep-water system in the offshore portion of the Talara Basin (Rossello et al., 2022). Overlying the Amotape Group are the following two shale units separated by unconformities: **i**) the Albian Muerto Formation that unconformably overlies the Amotape Group and consists of limestones and bituminous dark grey to black marls, originated in a mixed carbonate-siliciclastic environment in the Aptian, passing to more restricted environment during the Albian (Daudt et al., 2010), and **ii**) the Palaeocene Balcones Formation which is composed of distal shelf shales that rapidly onlapped the Redondo Formation (Daudt & Scherer, 2006). The Cretaceous deposition was controlled by normal faulting allowing arc-related sediment to reach the basin only during periods of subsidence in the forearc region (Dickson, 1995), possibly related to the plate rearrangement and/or seamounts colliding with the trench (Fildani et al., 2005, 2008). The few carbonate facies are restricted to parts of alluvial fan and fluvial conglomerates and sandstones of Cretaceous and Pliocene-Pleistocene ages (*e.g.*, Tablones Formation) (De Vries, 1988; Marsaglia & Carozzi, 1991; Carozzi & Palomino, 1993).

Tectonic setting

The most distinctive feature of the Talara Basin consists of a conspicuous configuration of structural highs and lows. These are expressed at different scales, as a product of a constant and diachronic uplift process with varying sediment supply from late Cretaceous to the present Andean tectonics (Palacios, 1994; Cobbold et al., 2007; Fildani et al., 2008). The depocenters are regionally distinguished by its configuration of highs and lows, defining structural blocks limited by fault arrays. Multiple structural lows are recognized (from South to North: Bayovar, Lagunitos, Malacas, Siches, Órganos, etc.), and the current depocenter of Tumbes, all which are separated by regional structural highs of Illescas, San Pedro, Paita, Negritos, Lobitos, Peña Negra-El Alto, and Banco Perú. The basement highs of the Amotape Group in the Illescas, San Pedro, Paita, Negritos, Lobitos, and Peña Negra - El Alto record diachronic uplift/tilting processes with different intensities over time to the present (Zeumann & Hampel, 2016; Llerena et al., 2018). This multiscale blocky configuration is clearly supported by outcrop, topography, bathymetry, seismic, gravimetry, magnetometry, well information, thermometry (Ro) analysis, and thermochronology data.

Although the Talara Basin is a world-class hydrocarbon producer, there has been controversy on defining its structural style for more than a century. Travis et al. *(*1976) and Higley (2004) considered it as a typical extensional basin with development of irregular blocks associated to purely extensional pattern of fractures, comparable to the appearance of broken glass. Nevertheless, Llerena et al. (2018) discarded the tectonic models classifying the Talara Basin (and other forearc basins in Peru) as extensional-type and postulated a forearc basin tectonic model with compressional deformation since the Eocene. These authors based their interpretation on i) subsurface surveys and dipmeter information, ii) paleo-bathymetric curves adjusted by biostratigraphy, iii) the analysis of sequences affected by erosion (uplift/ regression) and the identification of abrupt sea inlets (showing subsidence/transgression phenomena). In the same direction, Oviedo & Carlotto (2013) demonstrated the importance of compressional events in the evolution of the Talara basin recorded during the middle Eocene-early Oligocene due to the presence of surficial folded layers, reverse faults, thrusts, and associated sedimentary and tectonic breccias.

The integration of earthquake seismicity with surface GPS information (interseismic coupling) to understand the uplift and/or subsidence in the forearc, provides sense of current horizontal Andean deformation related to Nazca Plate subduction (Kelleher, 1972; Nocquet et al., 2014). The GPS studies have improved the understanding of crustal deformation processes and the seismic cycle, and also have allowed quantifying the position displacements of a point on the earth with accuracy in the millimetre to tenth-of-a-millimetre range (Figura 4B). Stern (2002) shows that approximately 1000 km-long subduction zone in Peru experiences low stress accumulation (Nocquet et al., 2014), therefore, plate convergence in the Wadati-Benioff region is accommodated mainly in an aseismic way where no large earthquakes (M >8.0) have been recorded for more than 5 centuries (Silgado, 1978).

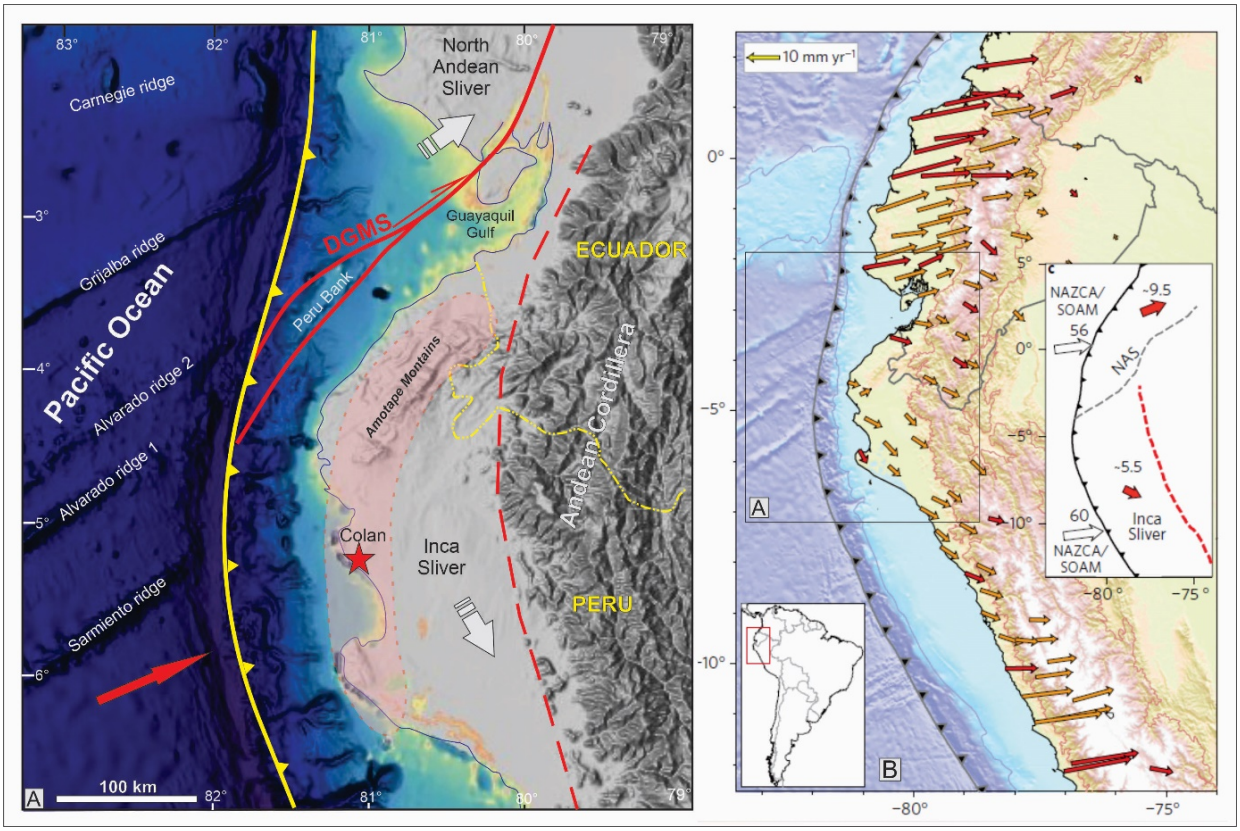

Figure 4. **A:** Morphostructural map of the NW Peru, showing the location of the Dolores-Guayaquil Dextral Megashear (DGMS), the trench, and the Inca and North Andean slivers. **B:** GPS velocity field with South America stable and plate margin kinematics with average motions of North-Andean and Inca slivers (taken from Nocquet et al., 2014).

The results reveal the divergent movement of two tectonic slivers of the South American plate: i) the North-Andean sliver in Ecuador and Colombia, and ii) a new tectonic sliver in northern Peru, which we have named " Inca Sliver ", moving at a rate of 9 mm/yr in the NE direction component and 6 mm/yr in the SE direction component (Nocquet et al., 2014).

Villegas-Lanza et al. (2016) evidenced to the north of Peru, through seismic coupling, that the horizontal stress near surface has NNW-SSE direction on the surface, parallel to the direction of subduction and different with respect to the regional subduction direction of the Nazca plate. This is interpreted being due to the effect of the Dolores Guayaquil Megashear (dextral), which causes a distortion of the current horizontal displacements on the continent south if it (Figura 4A).

The transcurrent-type deformations are evidenced with transpressive and transtensive sectors associated with related gravitational faults limiting the basal highs. The origin of structuring in the Talara Basin has been related to the interaction of: i) large underlying transpressional movements near the Wadati-Benioff-Nisqually zone between 60-90 km E of the trench (Pedoja et al., 2006; Witt & Bourgois, 2010; Zeumann & Hampel, 2016), and ii) ascending movements (generally abrupt, at rates of up to 4 mm/year), between 10-50 km E of the trench, produced by the subduction of the aseismic Sarmiento and Alvarado ridges (Zeumann & Hampel, 2016; Llerena et al., 2018). Fieldwork in the central part of the Talara Basin shows most of the faults measured in outcrop to be of transcurrent type, as supported by kinematic data (Murany, 1975). This is largely evidenced by subordinate kinematic indicators (*e.g.,* Riedel´s fractures, joints, etc.) that allow recognizing their character. Faulting is associated with a horizontal principal stress (σ_1) different from the current direction of subduction, only the 25% being normal faults (gravitational) and 5% corresponding to reverse faults (Oviedo & Carlotto, 2013).

Based on apatite fission-track data, thermal modelling, and geological data from the inner forearc system, Espurt et al. (2018) identified in the Amotape mountains the following two episodes of cooling/erosion/thrust exhumation: i) an older episode to the late Cretaceous (?) - early Eocene (~80 – 50 Ma) age, and ii) a youngest episode to the late Eocene - early Oligocene (36–27 Ma)-to-middle Miocene age. Both episodes correspond to periods of acceleration of the convergence rate, and those are separated by a period of strong subsidence, burial, and reheating

during middle-late Eocene (Norabuena et al., 1998; Nocquet et al., 2014).

Llerena et al. (2018) confirmed the current maximum horizontal stress direction NNW-SSE governing the upper section of the basin (between 1 and 5 km depth) and being responsible of the local structural regime in areas dominated by block uplift and/or subsidence. This observation is based on information of induced fractures and/or breakouts through image records in offshore wells. However, the stress direction differs from the subduction direction of the Nazca plate (~N 80°) recognized in Ecuador (Nocquet et al., 2014; Villegas-Lanza et al., 2016; Aizprua et al., 2019) and Peru (Villegas-Lanza et al., 2016) as possibly related to the stress field rearrangement produced by the Dolores Guayaquil Megashear. Maximum horizontal stress direction σ_1 resulting from kinematic analyses varies between NW-SE / NNW-SSE to N-S and it can be related to the direction of subduction ~N 80º to the middle Eocene-present (Jaillard et al., 1998, 2000). Seismic coupling studies show current horizontal stress in the shallow crust with direction NNW-SSE as a result of the rearrangement caused by the displacement of the dextral Dolores-Guayaquil Megashear (Villegas-Lanza et al., 2016; Chlieh et al., 2011; Chlieh 2014). It has been shown that the high-rank of active faults in the central part of the Talara Basin with an ENE-WSW direction are dextral in sense and their sinistral conjugates are disposed NNW-SSE, suggesting maximum horizontal compressive stress σ_1 with direction NW-SE (~N 130°). These transcurrent movements are verified by kinematic analysis of faults in surface and induced fractures/ breakouts in well images. This direction of compression differs from the present regional direction of subduction of the Nazca plate (~N 80°). The strike-slip component of the faults bounding the uplifted blocks are evidenced by applying this tectonic model to the seismic interpretation.

Apatite fission-track thermochronological data from rocks equivalent to the Amotape Group in Ecuador (Spikings et al., 2005), and from Palaeozoic schists in the Illescas hills (Wipf, 2006), show that the last uplift of these blocks began in the Oligocene and Miocene, respectively, and have continued to the Present. Bourgois et al. (2007) demonstrated by means of restitutions calibrated with 10Be data (Lal, 1991a, 1991b) that Cabo Blanco blocks in Peña Negra (Tablazo Formation), Paita, and Illescas (Palaeozoic) were islands by 200,000 years ago. Fildani et al. (2008), based on biostratigraphy, interpreted periods of abrupt subsidence and uplift during the Eocene through changes in the paleo-bathymetric curve. Thermal gradients based on vitrinite reflectance taken from outcrops and surface samples of various wells of remnant sedimentary sequences preserved in structural lows, demonstrated an erosion range between 2,000 and 3,500 m depending on the area (Pedoja et al., 2006).

Organic content in the Amotape Group

Several authors suggest that Cretaceous shales and limestones are the traditional petroleum source rocks of the Talara Basin, principally represented by bituminous marls of the Albian Muerto Formation and black shales of the Campanian Redondo Formation (Seranne, 1987; Zúñiga-Rivero et al., 1999a, 1999b; Arispe, 2001a, 2001b; Gonzales & Alarcón, 2002; Higley, 2004; Pozo-Calle & Castillo-Guzmán, 2018). In 1968, Grover Gonzales (cited in Prado-Paucar, 2018) indicated that Well 5237 drilled into the thicker section of the Amotape Group within the study area achieved 3,500 m. To the first 650 m, fine white to greenish quartzites were penetrated with presence of microfractures, followed by 1,000 m of dark grey to black limestone beds with traces of fluorescent material and containing some plant tissue and crinoid stems. A sample from the 2,300 m (more precisely at 6,900-6,930 ft) provided foraminifera identified as Staffella *sp*. and molluscs corroborating the assigned Pennsylvanian age. Below 3,400 m b.s.l., the traversed section shows a monotonous lithology of shales and argillites.

MATERIALS AND METHODOLOGY

The structural architecture of the studied area in the Colán Block was interpreted using a 2D seismic reflection survey acquired in 2015 (reprocessed in 2017) and calibrated by well data from several oil fields provided by Olympic Zeus. Seismic interpretation was conducted using the Kingdom platform. We reconstructed hydrocarbon generation and migration history using structural maps generated from seismic interpretation and geological data integrated into a georeferenced database. A conceptual geological model of the basin incorporating major faults, was developed based on 3D seismic interpretation and used to define the physical and temporal

inputs necessary to conduct the petroleum system modelling (Magoon & Dow, 1994).

To determine the petrophysical properties of different lithologies to the Amotape Group, we conducted field work, gathered representative samples, and made mesoscopic descriptions, based on a multi-scale methodology approach as described below. Specifically, depths of sampling for borehole information analyses are referred to in feet in order to keep high accuracy.

Micro-mesotectonic analysis of outcrops

These analyses were carried out in mesotectonic stations (Gross & Seelig, 2006) distributed as regularly as possible, including the constituting lithologies of the Amotape Group that crop out along cliffs and marine terraces south of Paita. Primary structural data (stratification, lamination, foliations, etc.) and those corresponding to structures (fractures, veins, etc.) were collected. We also performed quantitative measurements of structures intended to display them as stereographic diagrams of spatial relationships (Wulff network-type) and statistics (Schmidt network).

Structural analysis of FMI images and/or drill cores

Good quality image logs at 1:20 scale as well as borehole breakouts of some recently drilled wells have been analysed in order to reveal oriented structures. Also, determination of the linear density of fractures constituting this kind of unconventional reservoir system was performed.

Petrographic analysis

Thin sections with vacuum impregnation using high quality, low viscosity blue epoxy resin across the samples at a uniform thickness (25 µm) were prepared. Plucking was minimized and pores up to 1 µm in diameter were permeated making them more visible, therefore, thin sections were ready for an analysis of the pore system geometry. All thin sections were stained with alizarine red to distinguish calcite from dolomite and photographed. Forty-eight samples were chosen to individually classify clastic rocks following the terminology proposed by Folk (1974), and carbonate rocks according to the criteria of Dunham (1962). Porosity was determined to clastic rocks following the textural terminology of Schmidt & McDonald (1979), and to carbonates based on Choquette and Pray (1970).

Petrophysical study

Density, porosity and permeability have been measured under standard conditions in 17 samples according to the following steps: i) Collecting the samples to obtain a plug of 38 mm in diameter and 55-65 mm in length and cleaning them in Soxhlet equipment with toluene to remove hydrocarbons in aqueous phase and methanol to eliminate salts, ii) oven drying to constant weight using Automated Permeameter Porosimeter - Core Test Systems, Inc. to qualitatively determine the increase in secondary porosity associated to the density of fractures, and iii) determining the relative contribution of primary porosity through analysis of density-neutron and sonic porosity logs.

Electron microscopy studies (SEM)

Samples were dried at low temperatures for 3 days to prevent shrinkage of the clay minerals, and sprayed with gold forming a film that facilitates conductivity when the samples are bombarded with electrons, for better examination under the microscope. Ten samples have been analysed for porosity and pore throats to take the following values: abundance, tortuosity, pore size distribution, and pore classification to throat diameter ratio.

X-ray diffraction analysis

Using XRD qualitative and semi-quantitative determination of all mineral components, including clays and zeolites, was obtained. The mineral components of the whole rock were identified. For clay mineral analysis, three different tests were performed on each oriented sample: i) first natural test (air-dried decanted clays) was prepared to identify the main types of clays, ii) second test was performed on glycolated samples (exposed to ethylene glycol vapours) to determine the swelling capacity of the clays, and iii) third test was on the fine fraction treated and heated which, at 550ºC, gives the abundance of kaolinite and chlorite.

3D modelling based on seismic analysis of the unconformity sedimentary sequences-technical basement

A geomechanically 3D model for the Amotape Group was built using all the different collected subsurface data in order to identify the different deformational events associated to the Palaeozoic, Mesozoic and Neogene episodes. These episodes have their own responsible stress fields that are not necessarily coaxial, therefore, they were identified in time and space. The morphotectonic analysis expressed by the relative position of highs and lows blocks related to more or less competent lithologies, were conducted. Due to the resolution of the available seismic survey, fractures were hardly detected. However, the

faults distribution was probably linked to the secondary porosity framework using interpreted attributes, some marked horizons, and interval attributes correlating quite well with the better defined interbedded fractured facies of the Amotape Group.

RESULTS

The petrophysical characteristics of the Amotape Group were inherited from sedimentary protoliths consisting of intercalations of white, grey to black quartzites, hard argillites, and dark grey to black slates with lesser amounts of pyrite, calcite, and talc. The complete stratigraphic sequence is dominated by siliciclastic packages ranging in age from Palaeozoic to Upper Eocene, and mostly Quaternary. The Tablazo Formation is recognized from both onshore and offshore subsurface information, and by outcrop data. The surface is approximately covered by 90% of Pliocene marine terraces overlied by Quaternary sequences of the Tablazo Formation, exhibiting poor Cenozoic outcrops mainly restricted to existing streams. The true thickness of the Amotape Group in the Portachuelo field is unknown.

Field surveys

The main petrographic and structural characteristics of the outcrops studied on the coast south of the Paita city (Figure 1) are summarized. Although the measured structural data are non-systematic to build a consistent fracture model, it is possible to preliminarily sketch a diagram of stress field based on quartz veins distribution into leptometamorphites. Maximum horizontal principal stress is oriented following an ENE-WSW to sublatitudinal orientation. The metamorphic rocks of the Amotape Group exhibit an approximated north to south oriented anisotropy disposition with inclinations that oscillate between 50 and 60º, preferentially to the east (Figure 5). This stress field orientation would be quite close to the one related to the ongoing subduction.

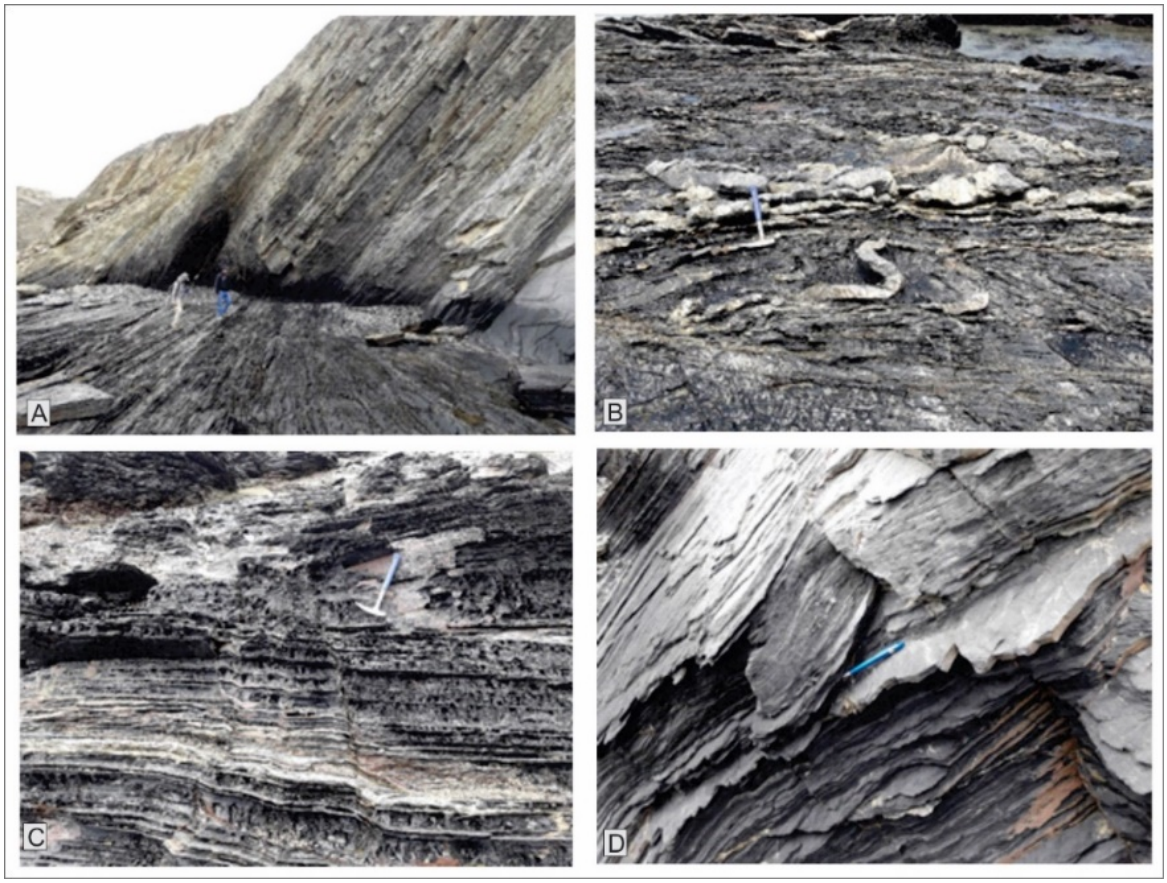

Figure 5. Outcrop view of the Amotape Group on the coast at west of Paita city, showing the regional disposition of strata dipping towards the west (A) and evidence of synsedimentary deformation from slumping and convolute stratification (B). Detail of the leptosedimentary rhythmic sequences of Amotape Group with interference cleavages at very fine levels (C). Detail of the leptosedimentary rhythmic sequences of the Amotape Group with slaty cleavages. Rhythmic sequences of carbonaceous slates interbedded with quartzites and phyllites. Note the monotonous alternation and parallel bedding (D). Detail of the syn-sedimentary dipping to NW caused by gravitational slides (convolute bedding) (E 482481 /N 9439136) west to Paita city (E 482836 /N 9438894).

Mesoscopic observations from outcrops of leptometamorphic parts of the Amotape Group in the ravines and abrasion surfaces of the coastal sector located west of Paita city, show regional ~N-S strike and ~45° dip towards the west. Some photographs of the main outcrops are shown below. Some very fine beds contain carbonaceous material (Figure 5). In La Silla hill (La Tortuga, east of Islilla) Triassic granites (220 ± 1.5 and 239 ± 2 Ma, Bellido et al., 2009) intrude metamorphites of the Amotape Group (Figure 6).

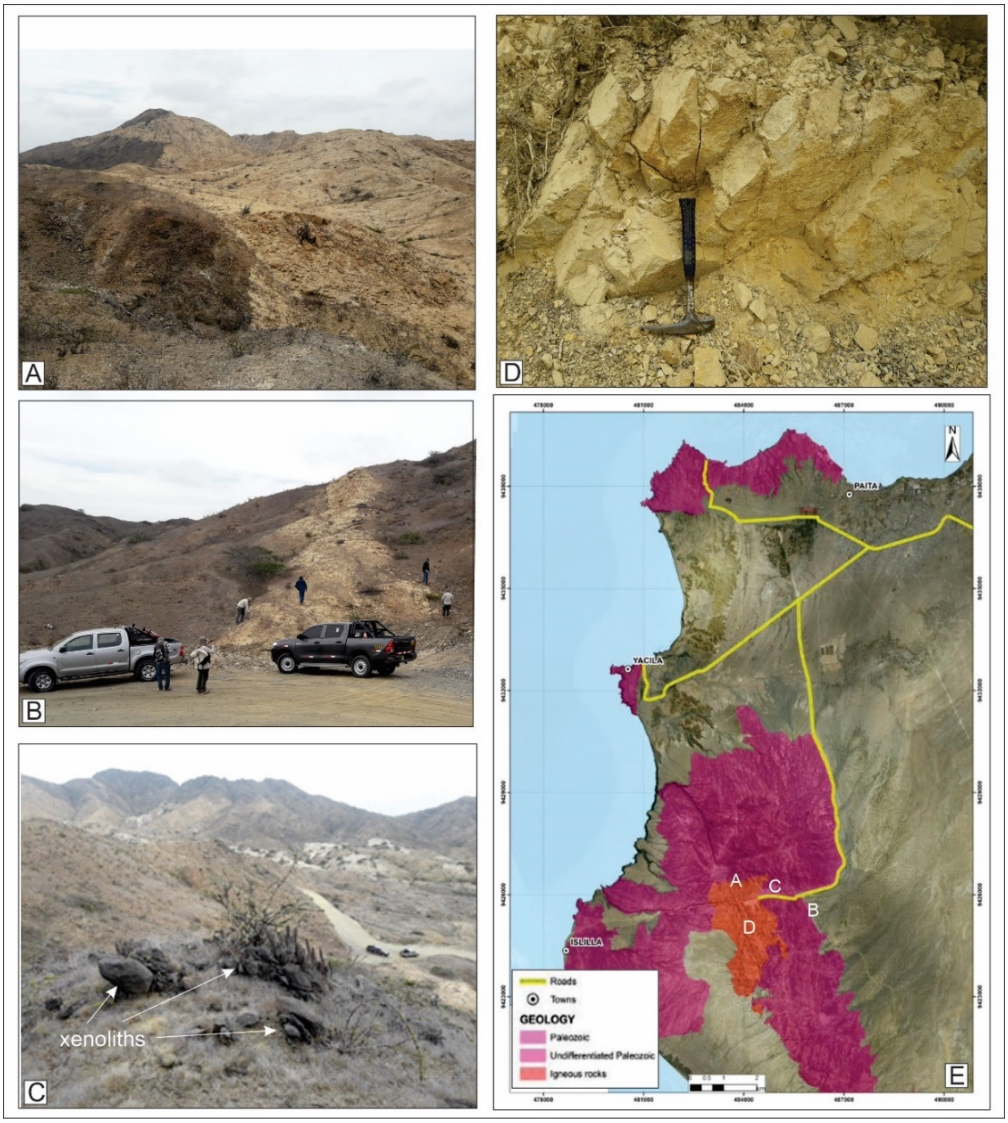

Figure 6. A: Intrusive contact between the granite and its leptosedimentary host rocks. Amotape Group **B**: View of a subvertical disposed granitic dike with general strike N 350º that exhibits late displacements due to faulting with transcurrent components. **C**: Xenoliths of the Amotape Group included into a granitic stock. **D**: Detail of fractures in the granite. **E**: Locations of pictures on theTriassic granite outcrops (modified from INGEMMET, 1999).

Siliciclastic strata attributed to the Mesozoic (probably Cretaceous, see Espurt et al., 2018) and containing thick conglomeratic levels are cropping out on the coastal cliffs and ravines south of Paita city (Figure 7). The succession is completed with sandstone strata and clast-supported conglomeratic lenses exhibiting imbrication that determines a general flow direction towards the NW. Some subangular, decimetric clasts in the conglomerate bodies display milky quartz veins like those encountered in the Amotape Group. In the canyons that descend towards the coast, and along the road joining Piura and Paita city, inclined Cretaceous sequences are totally pene-planated and locally superimposed by horizontal, ~1 m-thick, calcareous levels associated with the Tablazo Formation.

Quartz veins and fractures

The excellent quality of the outcrops of the Amotape Group along the coast, and the non-systematic character of the structural data measured over there on quartz veins and fractures, allowed us to preliminarily assess the stress field related to the lithological units containing them.

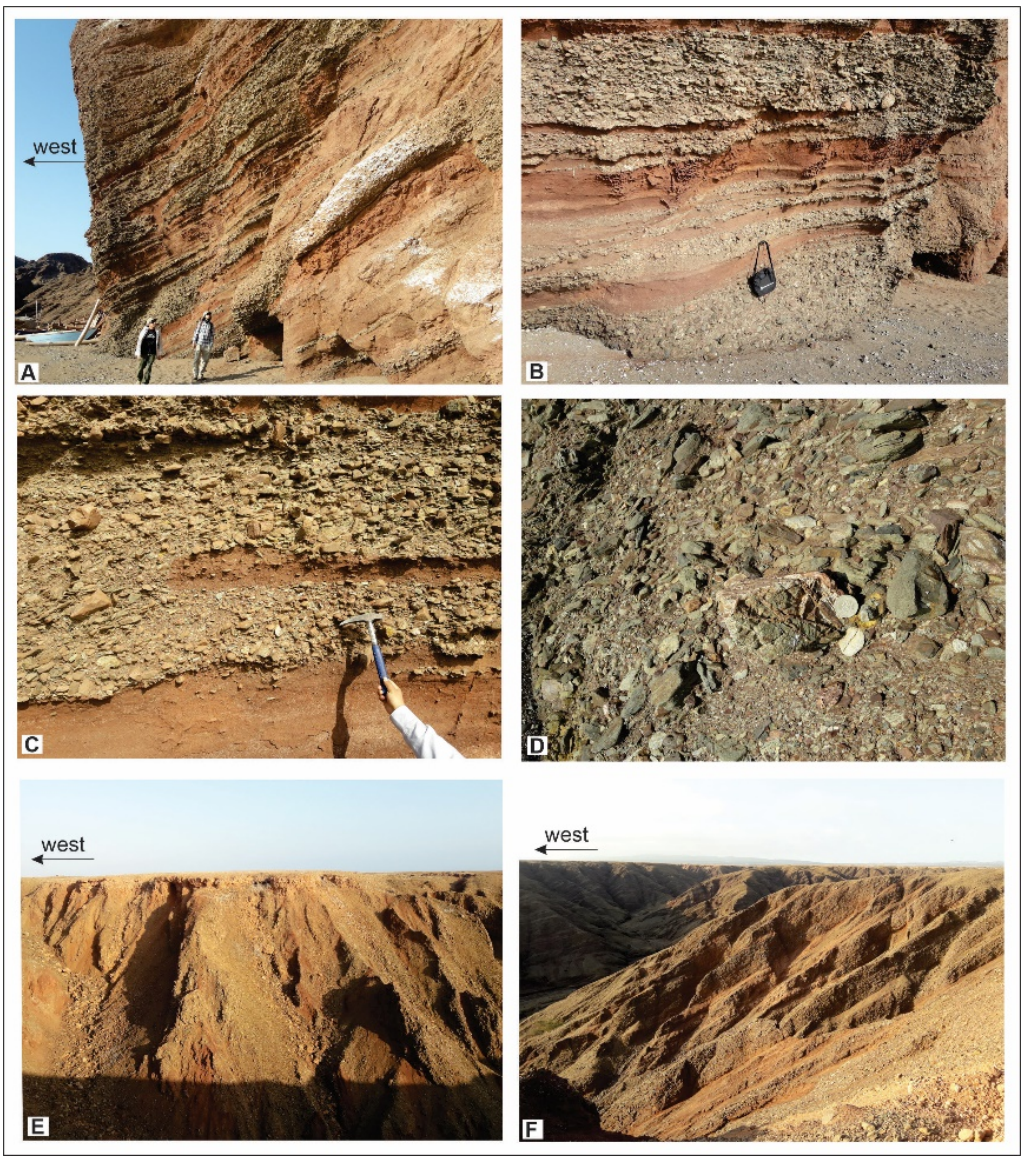

Figure 7. **A:** Siliciclastic sequences with conglomeratic levels attributed to the Mesozoic (probably Cretaceous), dipping towards west. **B:** Detail of the overlapping conglomeratic levels expressing a progradation direction towards NW. **C:** Detail of sub-angular and imbricated clasts typical of the Amotape Group Transport direction to the right. **D:** Detail of subangular metamorphic clasts of the Amotape Group exhibiting quartz veins. **E:** View of calcareous sub-horizontal sequences of the Tablazo Formation in angular unconformity and filling soft reliefs carved on the Mesozoic sequences. **F:** View of the peneplanated Mesozoic siliciclastic sequences tilted towards west.

As a consequence of this, an early event responsible for the opening of discontinuities that allowed the emplacement of the different veins in leptometamorphites and their later deformation was recognized. The regional late stress field respon-sible for the fracturing and veins was oriented with its maximum horizontal stress trending sublatitudinal to ENE-WSW strikes.

Multiple milky veins were generated by mechanical-metamorphic segregation, and these are related to the confining pressure conditions suffered by the hosted lithologies due to the burial load. Based on Riecke's Principle, confining pressure with dissolution phenomena have produced siliceous solutions from quartz grains. These solutions filled contemporaneously dilating subvertical fractures located into the most competent levels. The analysis of the morphological characteristics and spatial arrangements of the quartz veins intruding the Amotape Group respect to bedding, allowed us to recognize the following families:

a) Veins subparallel to bedding. These are very irregular milky quartz veins controlled by the preserved bedding of the leptometamorphites (Figure 8). Lenticular and globular veins with more competent character produce enveloping cleavage fitting the more competent irregularities into the leptosedimentary strata.

b) Veins perpendicular to bedding. The most competent sandy levels of the Amotape Group exhibit conspicuous milky quartz veins in

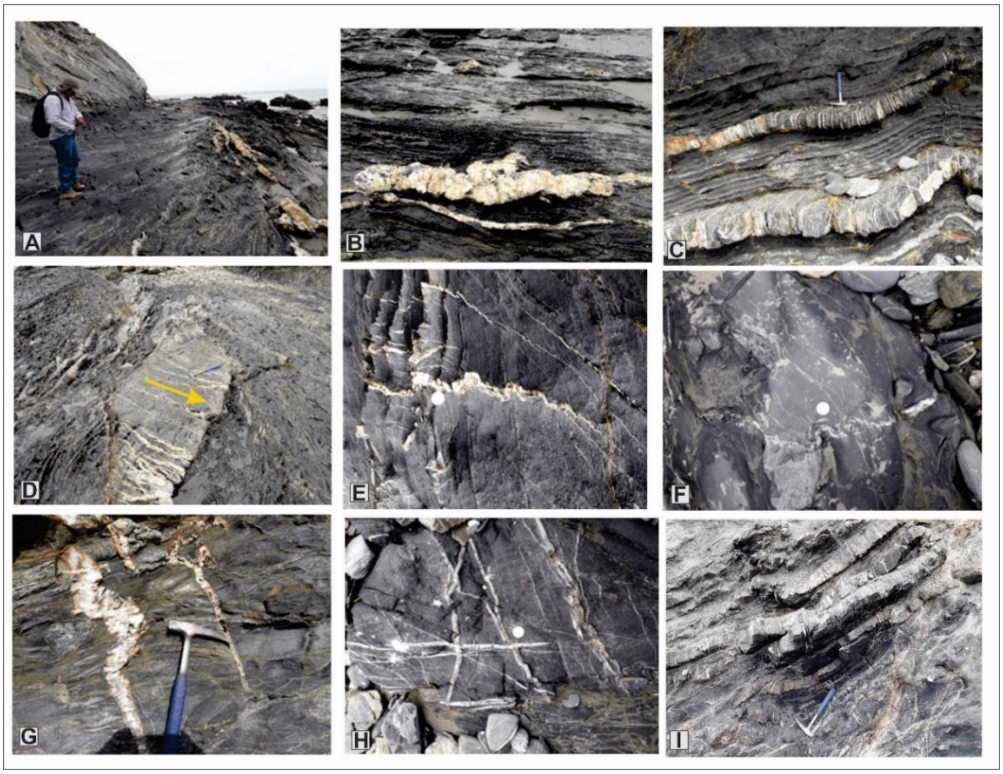

Figure 8. A: Venulations subparallel to discontinuities in the Amotape Group. **B:** Detail of lentiform and globose veins of milky quartz generated by metamorphic segregation. The relative competent character determines an enveloping cleavage of the leptometamorphites fitting them. **C:** Quartz venulation selectively emplaced sub-perpendicular to competent sandstone levels. **D:** The veins increase their power progressively from the lower contacts of the levels being intruded (yellow arrow). **E** and **F:** Subperpendicularly emplaced quartz venulation with ptygmatic folds with shortening on the order of 30-40% in the fine levels where they are emplaced. **G:** Detail of the earliest folded veins (left of the hammer) and other (right of the hammer) subparallel to the observation surface exhibiting incomplete fillings of limpid quartz with crystalline terminations, typical of dogtooth bands. **H:** Detail of intersecting quartz veins (coin as scale) **I:** quartz veins distribution on different competent levels.

arrangements perpendicular to the stratification (Figure 9C). These are thinner and their frequency is related to the thickness of hosting beds, which range between 10 and 50 cm. This type of quartz veins is preferentially located into hinges of the intraformational folded beds.

c) Deformed quartz veins. The action of subvertical maximum principal stress caused by burial compaction resulted in typical ptygmatic folded veins, shortened in some cases to 40% of their initial length (Figure 8). These features allow us to identify a mechanism of compaction simultaneous or subsequent to the intrusion of quartz veins. Even after this compaction, other veins are emplaced into undeformed beds showing incomplete filling characterized by geode sectors and crystallized bands with limpid quartz crystals showing dog-tooth textures.

d) Transcurrent structures. Thin quartz *en échelon* veins are arranged into elongated zones and creeping fold features determining transcurrent faulting affecting sequences of leptometamorphites (Figure 9). On sub-horizontal terraces carved by marine abrasion, sublatitudinally *en échelon* arrays of quartz veinlets with few meters long indicate sinistral wrenching. Outcrops with well-marked anisotropy trending N110º and dipping ~70º to the NE and/or ~50–60º preferentially to the east exhibit wrenching structures associated with drag folds in their surroundings (Figure 9).

e) Later joints. All the lithologies studied in outcrops exhibit fractures devoid of mineral fillings which affect the leptometamorphites. Also, these fractures affect different types of preceding quartz veins (Figure 10). In some cases, totally or partially open fractures with a mean opening between 1.5 and 0.25 mm are recognized. This type of fracture is very important in the characterization of the exploratory objectives because that joint contributes to the secondary porosity and permeability in the Amotape Group, especially in its uppermost part beneath the Meso-Cenozoic succession**.**

Petrographic studies of the Colán X139 well cores

The deeper segment of the Colan X139 well drilled 420 m and crossed different metamorphic rocks of the Amotape Group (Figure 11). From top-to-bottom the petrographic studies identified the following typical lithologies and fluorescent responses in the Amotape Group.

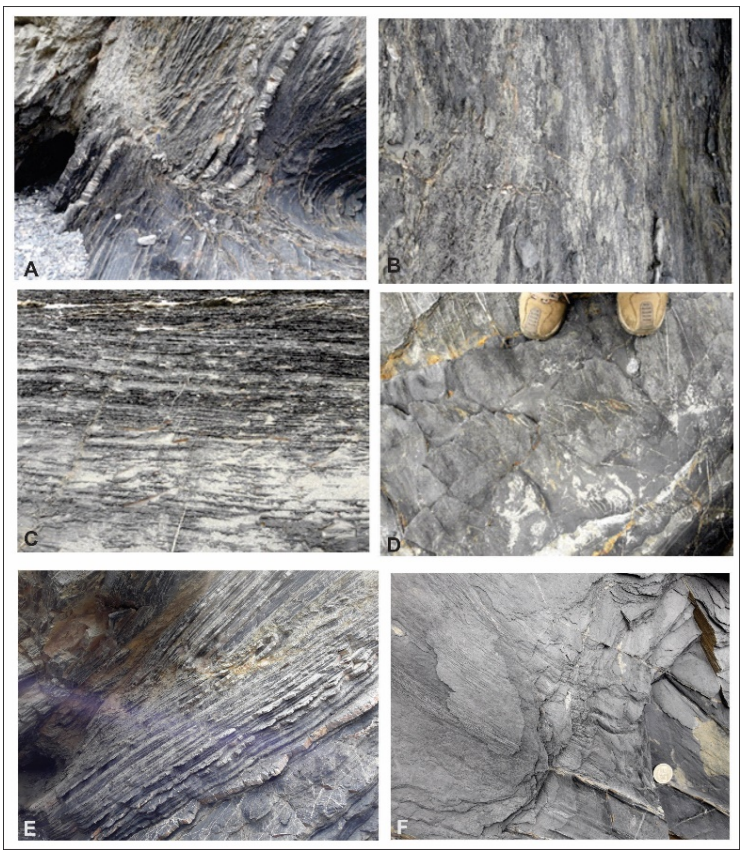

Figure 9. A: Detail of a late metamorphic transtensional fault disposed with strike N110º, 70º dipping to the NE, affecting a leptometamorphic sequence with approximate strike of N05º and dipping 55º to the NW. **B**, **C** and **D**: Details of left *en-echelon* trains of quartz veins indicating dextral syntectonic deformation disposed along sublatitudinal directions. **E**: bedding with convoluted structures. **F:** crenulation structures plunging towards west.

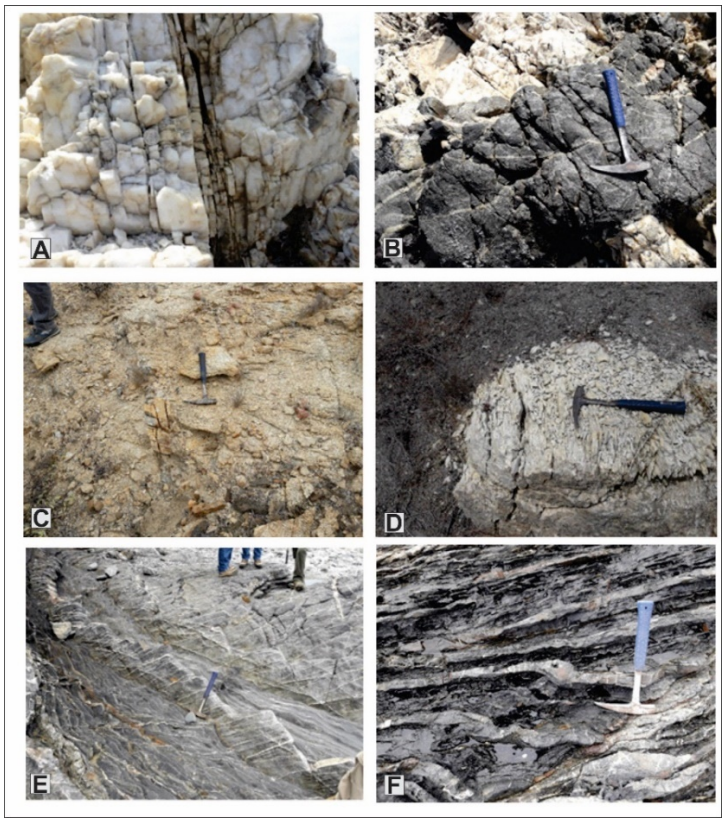

Figure 10. A: subvertical fractures developed in veins and quartz masses. **B:** Decametric subequidimensional outcrop of basaltic rocks included in the leptosedimentary sequences. **C:** Detail of multidirectional fracturing in granitic rocks. Preferably with milky quartz fill arranged N65º and N135º. **D:** Detail of the fracturing of quartz blocks into the Amotape Group. **E:** View of subhorizontal bedding surfaces showing the quartz veins perpendicular to the stratification cut by vertical discontinuities. **F:** Sigmoidal quartz veins interstratified into the Amotape Group.

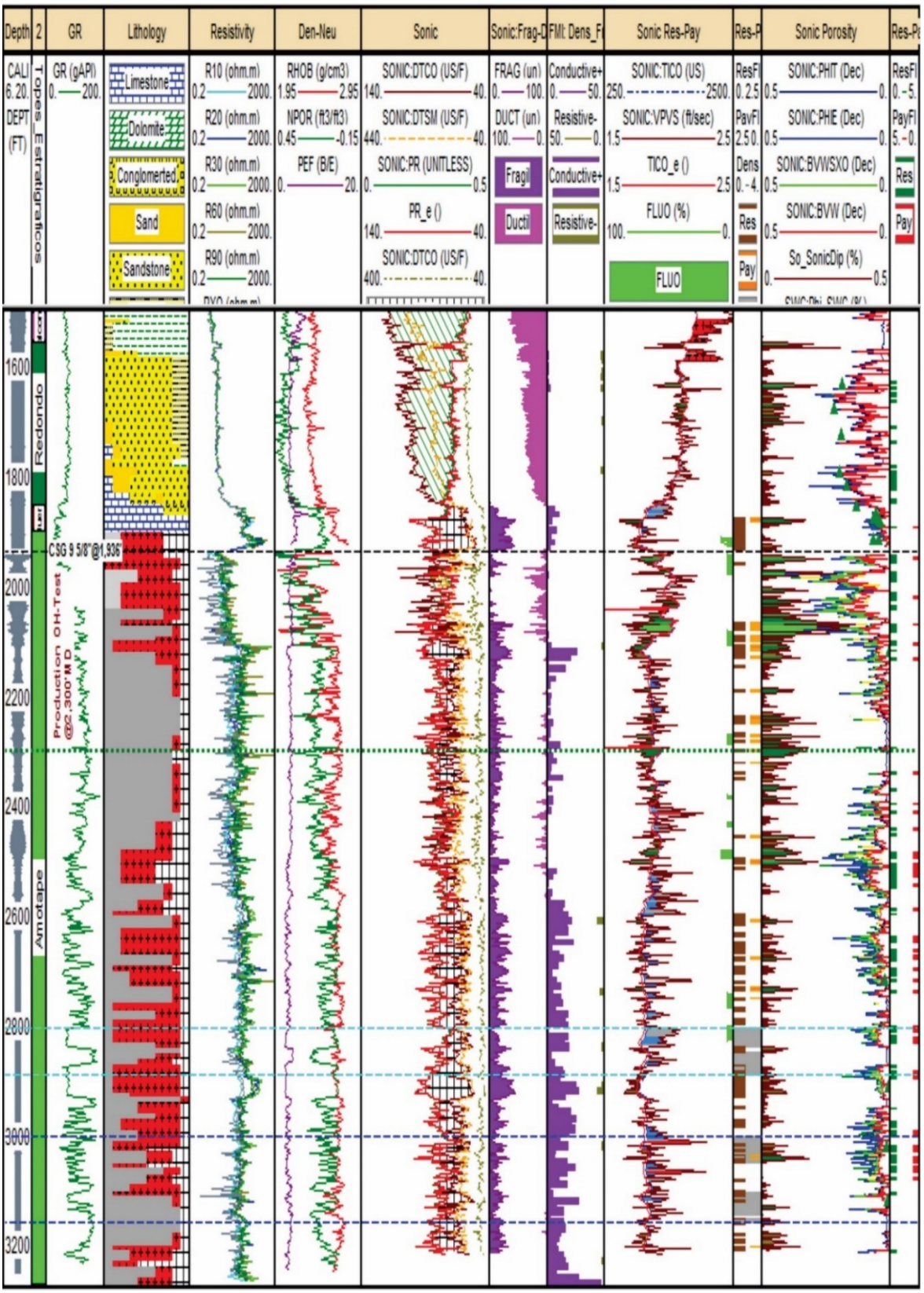

Figure 11. Lithological descriptions and petrophysical curves of the stratigraphic column crossed by the Colán X139 well. See references in the log header.

• ***Packstone/grainstone*** (1,915 ft depth, Figure 12a): These lithologies display a strong calcareous reaction and abundant bioclastic fragments, gastropods, and bivalves >2 mm in size. Fracturing exhibits sectors with the appearance of brecciated rocks. Some microstylolites with insoluble residue show dark brown hydrocarbon-filled fractures with light grey fluorescence.

• ***Dolomite*** (1,917 ft depth, Figure 12b): The dolomitic mosaics are partially replaced by calcite and no siliciclastic grains were observed. These show moderate calcareous reaction with

abundant fissures in various intersecting directions, filled with dark brown hydrocarbons showing medium light grey (N6) natural mineral fluorescence with scarce, pale yellowish white.

• ***Sandstone*** (2,121 ft depth, Figure 12c): These rocks of medium size grains with dominant lithoclasts show high compaction, no calcareous reaction, but subvertical microstylolite fractures. Also, there can be observed medium grey (N5) and dark grey (N4) natural and cut-off fluorescence (-).

• ***Metarenite/Cataclasite*** (2,669 ft depth, Figure **12d**): Correspond to metarenites affected by deformation, cataclasis, and recrystallization without calcareous reaction. Some of them exhibit high fragmentation due to fracture planes where quartz crystals and hydrocarbon stains can be identified, showing medium grey (N5), natural fluorescence (-), and scarce yellowish white cut fluorescence.

• ***Metarenite/Cataclasite*** (2,815 ft depth, Figure 12e): These metarenites are affected by deformation, cataclasis and recrystallization. Grains and crystals of very fine to fine size are recognized and calcareous reaction is absent. Sets of very thin subvertical sealed fractures are crossing the sidewall core plug. Quartz crystals are identified in an open fracture plane. Medium grey (N5), natural and cut-off fluorescence was identified.

• ***Metarenite/Cataclasite*** (2,875 ft depth, Figure 12f): This metarenite is affected by deformation. Fine- to very fine-grained cataclasis and recrystallization are recognized. Sets of very thin subvertical sealed fractures are crossing the core of the sidewall. Quartz crystals and hydrocarbon stains are identified in an open fracture plane. Medium grey (N5), natural and cut-off fluorescence.

• ***Metarenite/Cataclasite*** (2,913 ft depth, Figure 12g): This metarenite is affected by deformation. Cataclasis and recrystallization with an abundant to moderate content of grains and fine to medium sized crystals are recognized. No calcareous reaction was reported. Sets of very thin subvertical sealed fractures are crossing the sidewall core and exhibit medium grey (N5), natural and cut-off fluorescence.

• ***Metarenite/Cataclasite*** (2,921 ft depth, Figure 12h): This metarenite is affected by deformation, cataclasis and recrystallization. Very fine to fine grains and crystals are differentiated and calcareous reaction is absent. A subvertical, black, soft (coal?) discontinuous band with 2 mm thickness is observed, showing an irregular dark halo around it with medium grey (N5), natural and cut-off fluorescence.

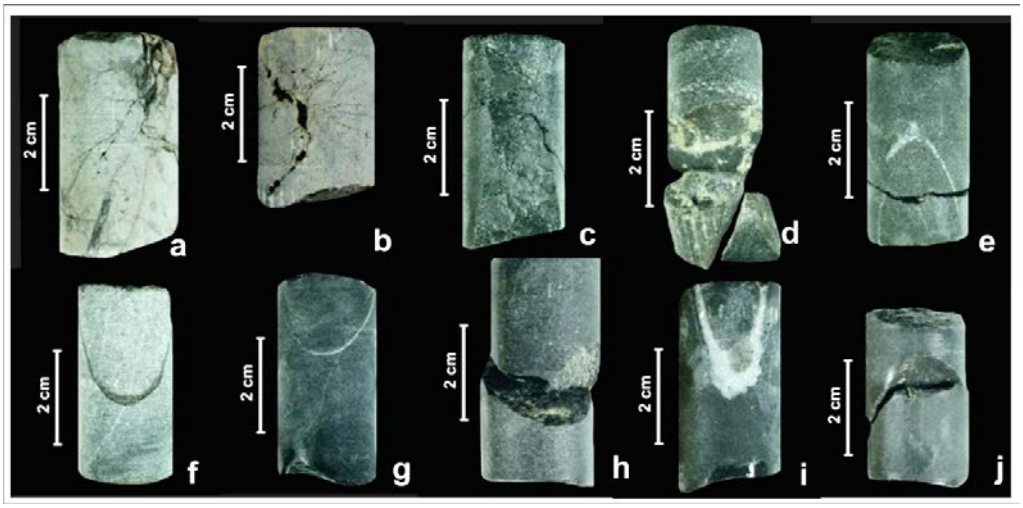

Figure 12. Petrographic studies on Colán X139 well. **a**) Packstone/grainstone (1,915 ft). **b**) Dolomite (1,917 ft). **c**) Sandstone (2,121 ft). **d**) Metarenite/Cataclasite (2,669 ft). **e**) Metarenite/Cataclasite (2,815 ft). **f**) Metarenite/Cataclasite (2,875 ft). **g**) Metarenite/Cataclasite (2,913 ft). **h**) Metarenite/Cataclasite (2921 ft). **i**) Metarenite/Cataclasite (3,113 ft). **j**) Metarenite/ Cataclasite (3,215 ft)..

• ***Metarenite/Cataclasite*** (3,113 ft depth, Figure 12i): This metarenite shows deformation, cataclasis and recrystallization. Very fine to fine grains and crystals are differentiated. A fracture filled with quartz crystals and pyrite is observed. This rock exhibits medium grey (N5), natural and cut-off fluorescence.

• ***Metarenite/Cataclasite*** (3,215 ft, Figure 12j): This metarenite is affected by deformation, cataclasis and recrystallization with differentiated fine grains and crystals. Few 1 mm-wide open fractures with white crystalline cement but without calcareous reaction. This rock shows medium grey (N5), natural and cut-off fluorescence.

The original sedimentary characteristics of all samples analysed of the Amotape Group, such as grading, packing, grain size, grain shape, and roundness, have been modified by deformation and recrystallization **(Figure 13**). These changes include diagenetic features of secondary overgrowths of quartz and feldspar, which have been partially erased by grinding, cataclasis, and recrystallization, only leaving relicts in sectors of some samples.

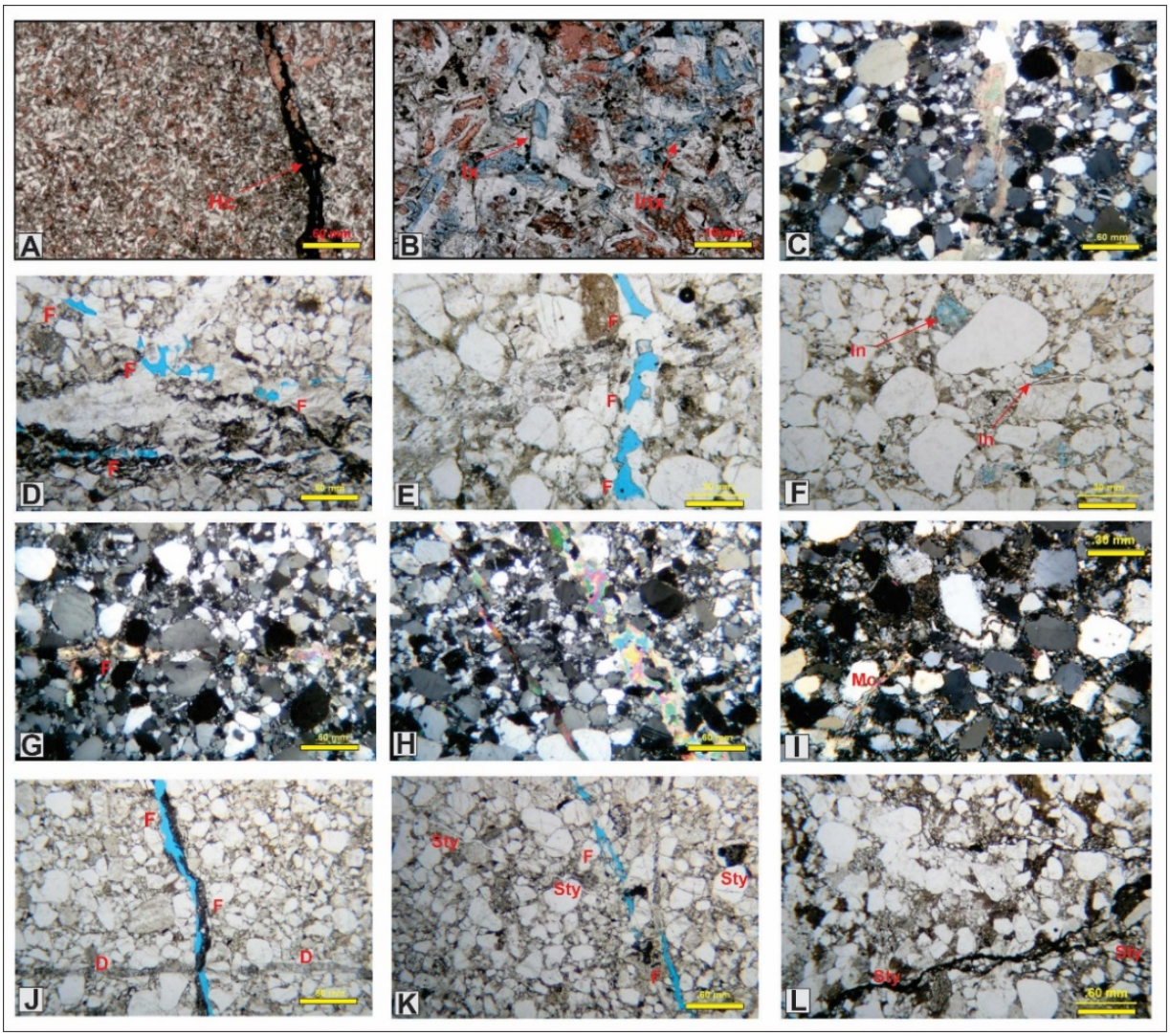

Figure 13. Microphotographs of petrographic sections of Amotape Group. sandstones. **A**) Sample (1917 ft) of dolostone. Fracture filled with calcite and stained with hydrocarbons (Hc). Parallel nicols. **B**) Sample (1917 ft) dolostone. Intracrystalline (Inx) and intercrystalline (Ix) porosity. Parallel Nicols. **C**) Sample (2913 ft) dolomite-filled fracture (F). Crossed nicols. **D** and **E**) Sample 2875 ft: partially open fractures (F), with quartz crystals as partial filling. Intercrystalline pores (Ix), among quartz crystals of fracture filling. Parallel Nicols. **F**) Sample (2719 ft). Intragranular pores (In), due to feldspar dissolution. Parallel Nicols. **G)** Sample (2913 ft) dolomite-filled fracture (F). Crossed nicols. **H)** Subparallel or stepped fractures (F), filled with quartz and later dolomite. Crossed nicols. **I**) White micas (Mc) originated by recrystallization and reorientation of detrital micas. Crossed nicols. **J**) Sample (2913 ft) meta-arenite / cataclasite. The grain size and shape as the granulometry distribution or presence of sedimentary structures are disturbed. A partially open fracture (up to 0.10 mm aperture) filled with microcrystalline dolomite cuts subparallel fractures filled with coarser dolomitic mosaics (D). Development of incipient discontinuous stylolites. **K**) Sample (2875 ft) meta-arenite / cataclasite. The grain size and shape as well as the granulometry distribution or presence of sedimentary structures are disturbed. Development of subparallel stylolites (Sty). Multiple fracture and filling events are recognized. **L**) Sample (2121 ft) litharenite disturbed by compaction. Development of zones of deformation and reorientation of grains, and stylolites (Sty) with concentration of carbonaceous material.

SEM studies

Different SEM studies on rocks of the Amotape Group were performed by LCV (2019) in the Colán 139X well, showing metarenite/cataclasite lithologies with fine to medium and subordinate very fine grain size, affected by brittle deformation. Also recrystallized and deformed sandstones with medium and subordinate fine particle size and moderate sorting were described (Figure 14).

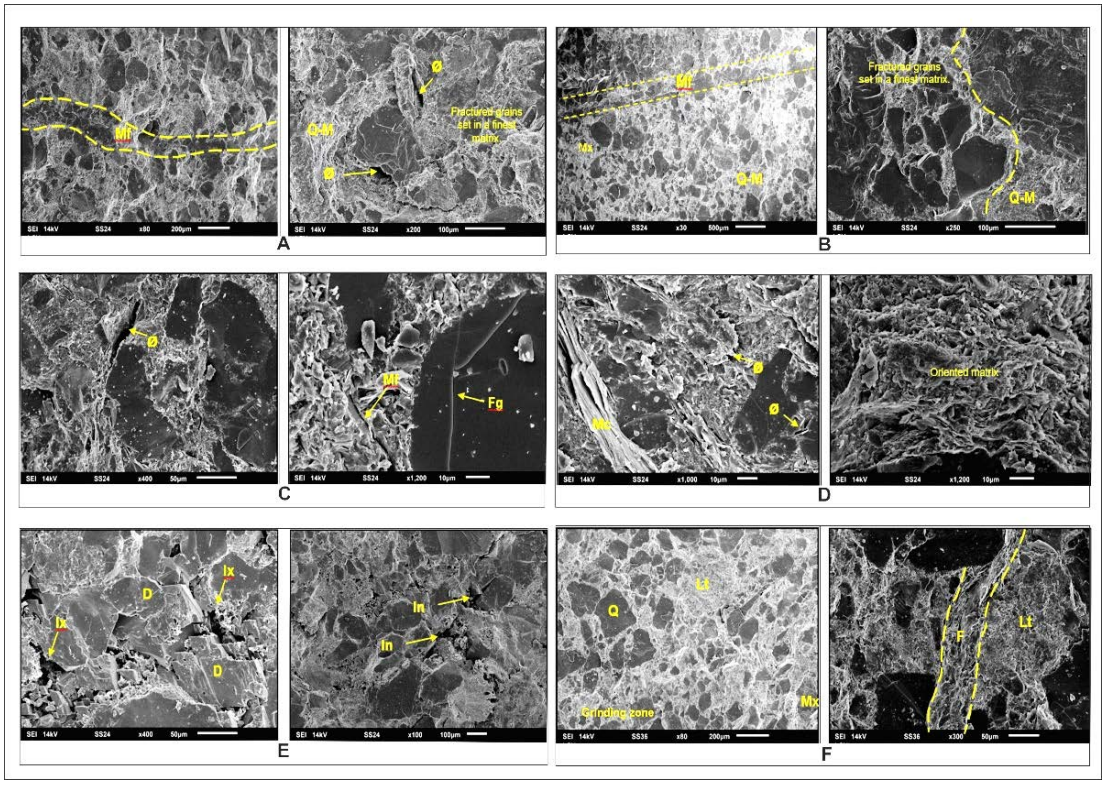

Figure 14. SEM studies on the Amotape Group from the OLY-COLÁN-XIII-5-139X samples (taken from LCV, 2019). **A)** Sample (3023 ft) meta-arenite / cataclasite with fine to medium and subordinate very fine grain size, affected by fracturing, deformation, and recrystallization. Continuous and deformed microfissure (Mf) filled with quartz, where grains are highly fractured and crushed, development of quartz-micaceous (Q-M) tails. **B**) Sample (3120 ft) ídem before, where grains exhibit irregular edges and are set in a recrystallized and deformed fine matrix (Mx), made up of clays, micas and quartz. Continuous fractures and microfissures (Mf) and the development of quartz-micaceous (Q-M) oriented and deformed incipient tails. **C)** Sample (2913 ft) ídem before, with deformation zones with abundant fractured grains (Fg) and grinding with irregular pores related to deformation zones, discontinuous open microfissures (Mf). **D**) Sample (2885 ft) ídem before, with irregular pores related to deformation zones, open discontinuous microfissures and mica cleavage (Mc). **E**) Sample (2719 ft) idem before, with grains present irregular edges and are set in a recrystallized and deformed fine matrix, made up of clays, micas and quartz crystals and cement represented by dolomite/ankerite (D) and secondary quartz overgrowth. Intragranular pores (In) by grain dissolution and presence of intercrystalline pores (Ix) among dolomite rhombs, subordinate intra cement pores generated by dissolution of dolomite rhombs. **F**) Sample (2121 ft) deformed litharenite with a medium and subordinate fine sand-sized arenite, with moderate sorting and dominant lithoclasts (Lt) and subordinate quartz (Q). A cut and deformed fracture (F) filled with quartz is observed.

These petrographic images evidence siliceous cement including the early clay coating. The quartz grains exhibit irregular edges and are embedded in a recrystallized and deformed fine matrix made up of clay, mica, and quartz, affected by fractures, brittle deformation, and recrystallization. In those sectors where grains are highly fractured, crushed and stretched, it is possible to recognise the development of incipient quartz-micaceous tails oriented and deformed. Microfissures continuous and deformed, filled with quartz, are highly fractured and crushed with quartz-micaceous tails and aligned inclusions. The porosity (ø) is low with hetero-geneous distribution of irregular pores, showing zones with greater cataclasis associated to microfissures located between the cleavage of micas and in the edges of rigid grains. This porosity is related to micropores from 1.56 to 27.16 µm, subordinate mesopores of 4.69 to 8.77 µm, subordinate micropores from 1.5 to 3.76 µm, and intragranular pores by grain dissolution. Some discontinuous microfissures have apertures from 1.8 to 41.40 µm, but in general, no porosity by pore throats is observed under the SEM.

The grains possess very irregular edges no matter if these were recrystallized or deformed, and these show varying sizes due to granulo-metric mixing by cataclasis and grain size reduction by grinding. The grains also appear fractured, crushed and/or stretched rearranged by rotation and exhibit inclusion trains, indicating grain fractures that were sealed. A microcrystalline to cryptocrystalline matrix between the grains is observed in which filling quartz has optical continuity with the surrounding grains. These have low content of clay minerals and fine whitish micas recrystallized in the cataclastic matrix that can produce incipient quartz mica tails

in the clasts. Very few coarser subhedral to euhedral, oriented white micas probably originated from recrystallization, and well reoriented, stretched or deformed detrital micas, are recognized. Some samples evidence the development of incipient and discontinuous stylolithic surfaces with homogeneous distribution. Also, isolated, continuous, well-developed stylolithes are generally cutting highly subordinate fractures

• ***Carbonate rocks.*** Sample 1,915 ft depth corresponds to a packstone/grainstone (bioclastic) and sample 1 at 1,917 ft depth to a dolomite. The packstone/grainstone (bioclastic) has a brecciated texture with abundant irregular fractures filled with calcitic mosaic, some of them displaced. Grains: 8% siliciclastic (predominantly monocrystalline quartz) and 60% carbonate (predominantly valve fragments, common gastropods, echinoderms and foraminifera). Matrix: 15% calcimicrite, partially with granulated texture. Cement is 15% calcite (sparitic mosaic replacing/ filling bioclasts, and fine mosaic recrystallizing bioclasts). The secondary porosity is low (2%), with heterogeneous distribution of the open irregular microcracks with 0.02-0.05 mm opening. The petrophysical data determines 6.61% porosity and 1.45 mD permeability. The dolomite shows a high degree of replacement forming a 60% of dolomitic mosaic that masks the original components, and planar-s with a flat subhedral texture. The dolomite crystallized diamonds are between 0.05- and 0.18-mm size. Abundant calcite (30%) as a dolomitic-mosaic replacement and as a filler for intercrystalline pores (between dolomite rhombuses), and moldy clay-filled pores are also recognizable. The secondary porosity is low (3%) with heterogeneous distribution of selective dominant intercrystalline (20%) and intracrystalline (60%) micropore size. Subordinate and non-selective open irregular microcracks (20%) with 0.02 mm opening are filled with calcitic mosaic and stained with hydrocarbons. Calcisparitic mosaic is observed replacing matrix and dolosparitic mosaic. The bioclastic calcite filling and dolomite lozenge replacement show intercrystalline pore filling. The dissolution of intracrystalline pores generates skeletal grains with moldy pore filled by clays and compaction-solution of seams and stylolithes. The petrophysical data determine 4.62% porosity and 0.52 mD permeability.

• ***Meta-sandstones*** (sample 2,121 ft)**.** These correspond to medium to fine sandstones composed mainly of soft lithoclasts, highly deformed by compaction. Stylolite and fracture development are observed. The clasts (94.5%) are of medium size, with subordinate fine sand, and these are represented by 72 to 75% lithoclasts, almost exclusively metamorphic (slates, phyllites, quartz and siltstones and fine recrystallized quartz-micaceous arenites, quartzose phyllites, metaquartzites), 20-25% mono- and polycrystalline quartz (quartz mosaics), and 3-5% of feldspars (plagioclase and indeterminate). The rocks possess 5% of pseudo-matrix with 0.5 to 2.5% of cement. Porosity is low (0.5%) and shows heterogeneous distribution represented by pores related to a microcrack.

• ***Cataclastic meta-sandstones*** (samples 2,875, 2,893, 2,913, 3,023 and 3,113, 3215 ft). These are very quartzitic samples, with signs of deformation by cataclastic flow and subsequent associated to fractures strongly recrystallized. In some of them recrystallization is dominant, while in others cataclastic deformation is dominant. Deformation bands are distinguished in all the samples, with greater evidence of grinding and/or recrystallization. Diagenetic features have been mostly erased by deformation and recrystallization. The early compaction modifies the recrystallized clays as grain linings. Secondary quartz overgrowth is very rare and is only visible in the recrystallized quartz grains, clays and micas associated with cataclastic flow. The dissolution affects the feldspars and lithoclasts and generates scarce intragranular and moldy pores. Siliceous cement occurs as sparse quartz mosaic in sample as fracture and pore filling. Later compaction forms stylolithes and fractures filled with quartz or microcrystalline dolomite, and rare anhydrite as pore filler.

Colán X139 well imaging

The Colán X139 well was drilled subvertically (maximum deviation of 2.1 degrees, Figure 15). FMI-MSIP images were acquired in the Amotape Group between 1,938 and 3,274 ft depth. Throughout the well, the main discontinuities correspond to sharp lithological changes expressed by generally subhorizontal resistive responses. Some sections however show slight changes in the dip direction, preferentially to the west. These lithological changes are related to interfingering with thickness in the order of 5 to 10 cm of sandy resistive levels with pale yellowish tones and pelitic conductive levels with darker brown tones.

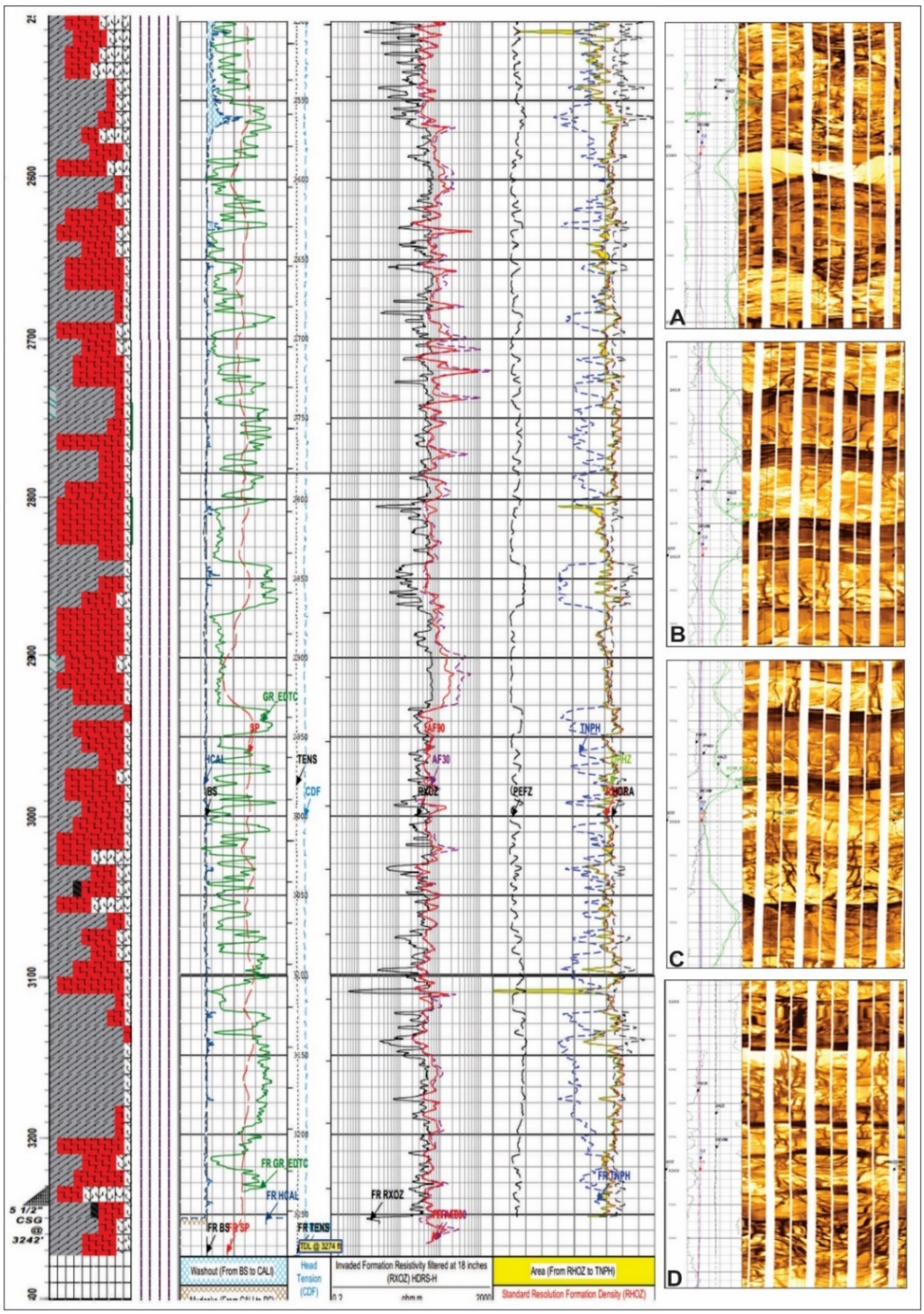

Figure 15. FMI image captures from the Colán X139 well showing the main types of subparallel and orthogonal discontinuities in the Amotape Group. **A**: Detail of a quartz vein subparallel to the stratification. **B**: strong resistive contrasts determined by the rhythmic alternation of originally sandy and pelitic lithologies. **C** and **D**: concentration of fractures along subvertical bands arranged at 180° in a NE-SW direction that would be compatible with the expression of borehole ovalization (break-out).

The most evident fractures are subvertical with little development associated to the bedding thickness of more competent lithological levels. These propagate from the contact with more pelitic levels and are progressively thinning out towards the opposite boundary until they completely disappear. The most frequent orientations strike NE-SW. Other fractures with irregular surfaces arranged in subparallel or staggered bands of the open type are present due to harder and resistive infilling material (quartz and/or calcite). Features compatible with breakouts are not observed, although the greater concentration of subvertical bands of fractures arranged at 180° with NE-SW strikes could correspond to those (Figure 15).

Subsurface data

Based on the seismic surveys, well logs, transects and structural mapping carried out in the studied Colán sector, we recognize main morphological 10 to 100 m-sized features. The Colán X139 well reached the top of the Amotape Group on the western flank of the basement corridor cropping out at the Amotape and Silla de Paita mountains that are progresssively onlapped by thinning Cretaceous strata (Figure 16A). This well shows clear correlations of the sedimentary sequences of the Muerto, Redondo, Balcones, Salinas, Palegreda and Chira-Verdum formations overlying the Amotape Group. The wildcat No. 4610 (the first oil discovery in the Amotape Group), was located on the northeast edge of the Portachuelo high towards the NW of the studied area (Prado-Paucar, 2018).

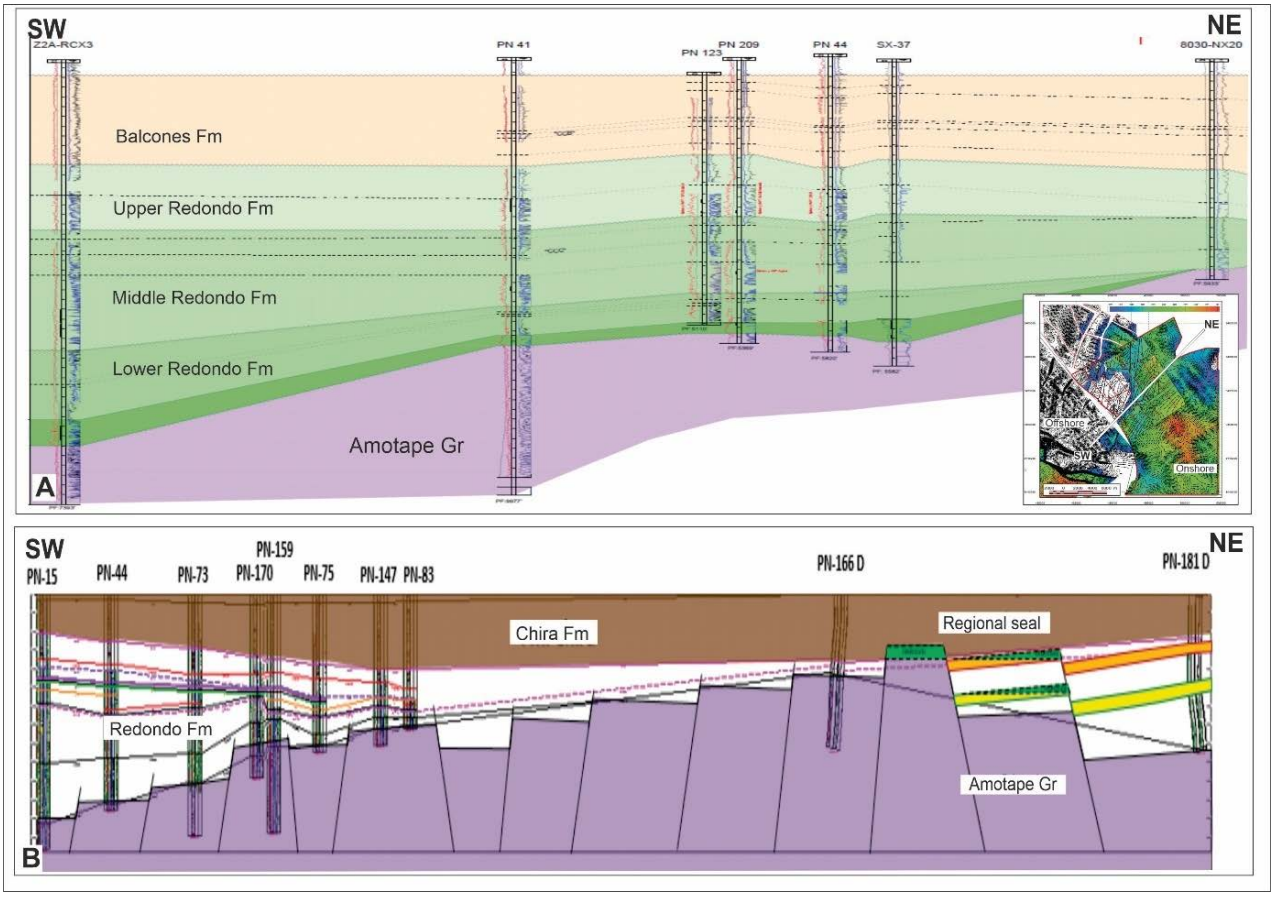

Figure 16. A: Transect controlled by well showing sedimentary sequences overlaying the western flank of the Amotape Group basement high. **B:** Schematic transect showing the fault pattern affecting the Amotape high located in C. (see location in **Fig. 1**) (courtesy of Zeus Energy).

South of Paita, a seismic survey imaged a series of staggered minor highs of the Amotape Group with a general NNE-SSW orientation suggesting left-lateral transpression (Figure 17). According to the interpretation of the available subsurface data and the regional context, it is possible to recognize the succession of two deformational episodes responsible for the fractures in the Amotape Group: **i**) a first extensional episode particularly active during the Eocene and characterized by the development of N-trending normal faults dipping to the west (Figure 17A), and **ii**) the second, Neogene transpressional episode, characterized by NNE-trending structural high and forming a broad fold with a tendency to observe double plunging axis with subordinate culminations and anti-culminations (Figure 17B).

The fracture distribution, probably related to secondary porosity, is barely detected in seismic images. However, interval and horizon attributes correlate well with the best production objectives into the Intra-Amotape Group facies. The Average Negative Amplitude H-H250 ms of the SW attributes, with values below -2,500 are related to discontinuities that indicate porosity variation, and values below -5,000 are related to lineaments that may be associated with fracturing.

Different transects based on seismic sections through the high formed by the Amotape Group evidence onlapping truncations of the overlying Cretaceous-Tertiary sedimentary strata (Figure 18).

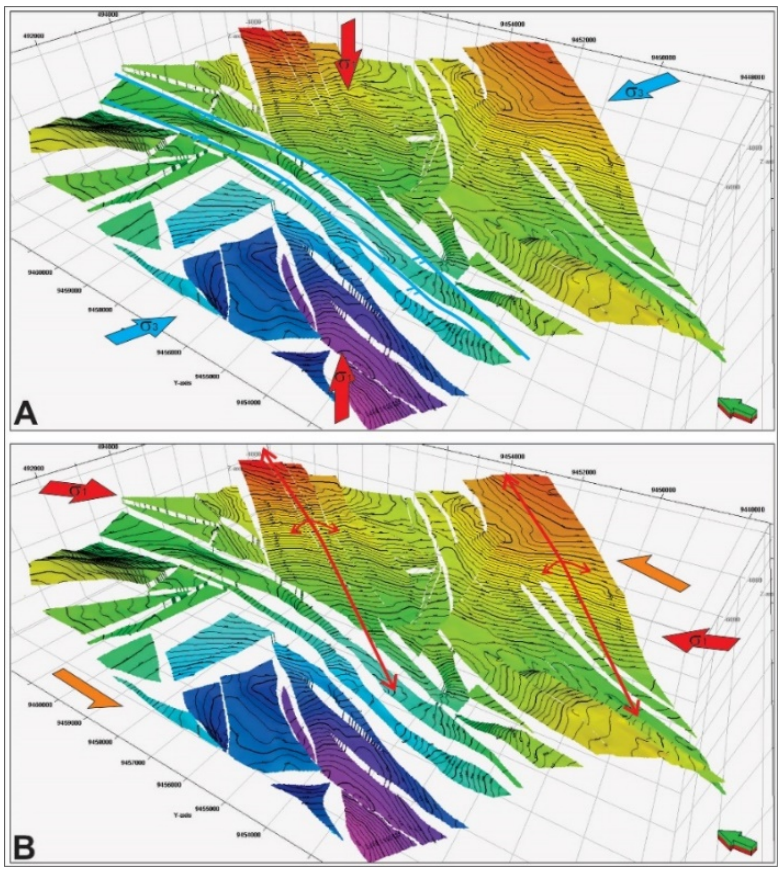

Figure 17. Schematic evolutionary model to the near-top of the Amotape Group. **A**: Shows N-S normal fractures dipping towards west due to an early extensional tectonic episode. **B**: NE-SW subordinate folding axe due to a late sinistral transpressive episode.

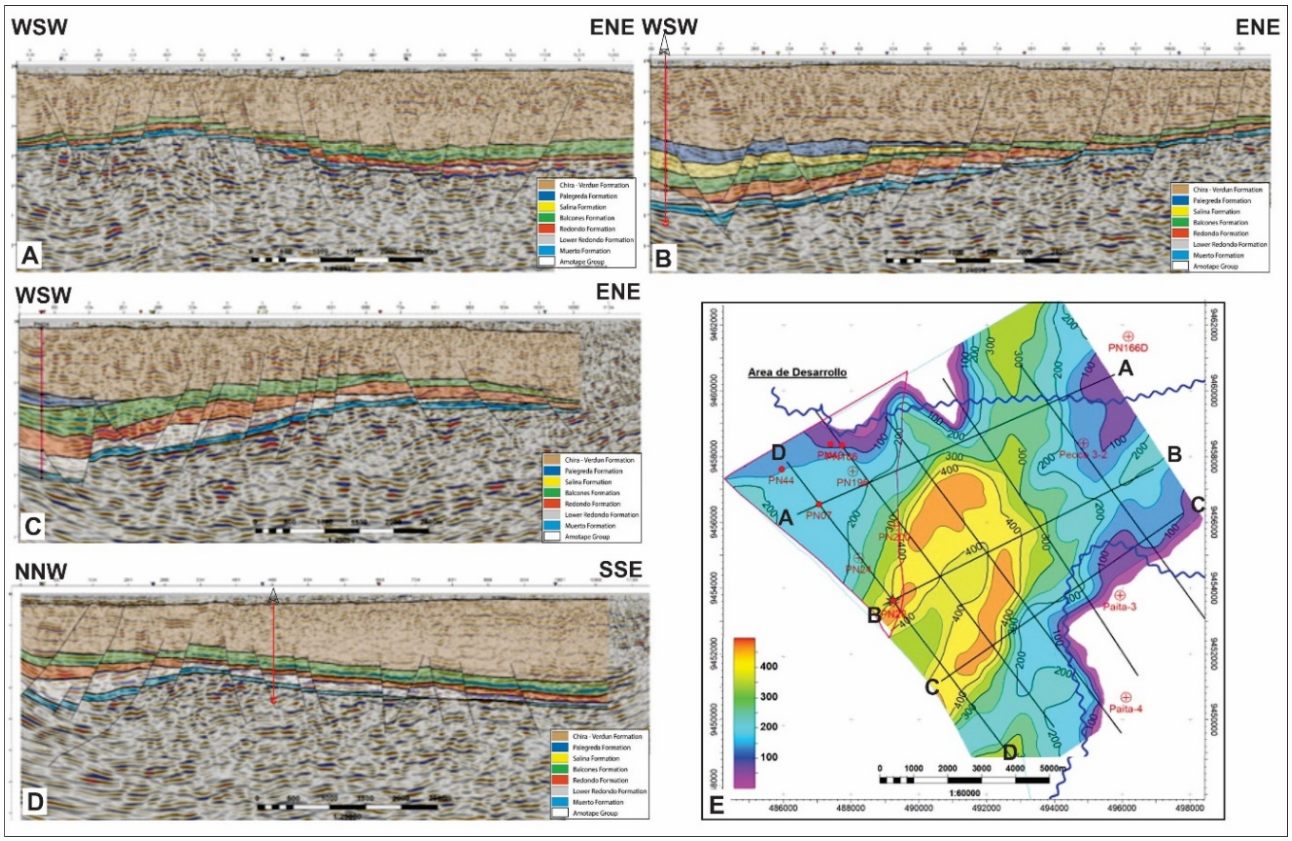

Figure 18. A, B, C and **D**: Transects showing the position of exploratory and producing wells through a basement high constituted by the Amotape Group (see location in **Fig. 1**). 1: Amotape Group., 2: Muerto Formation., 3: Lower Redondo Formation., 4: Upper Redondo Formation., 5: Balcones Formation., 6: Salina Formation., 7: Palegreda Formation., 8: Chira-Verdum Formation. **E**: Structural map at the top of the Amotape Group.

The planar anisotropies in the Amotape Group are expressed by bedding and/or metamorphic cleavages generally having strikes of 10° to 40° E, dipping between 40° and 60° to the northwest. Only 25% of the faults corresponds to gravitational faults and 5% to reverse faults where these determine a configuration of structural highs and lows from the Late Cretaceous to the present. Dinitz et al. (2010) evidenced transcurrent-type deformations with transpressive and transtensive sectors associated to gravitational faults limiting the basement highs. These faults respond to a stress field active during the Lower Eocene with NW-SE direction of their maximum horizontal stress (s_1). The stress field changed to NE-SW during the Middle Eocene and later to NW-SE during the Upper Eocene.

Model of geological evolution

An evolutionary model of the upper portion of the Amotape Group has been proposed to the interval 540-56 Ma (Figure 19). From an initial stage of peneplanated basement to the Amotape Group (Figure 19A), the beginning of subsidence controls the sedimentation of the Muerto Formation (Figure 19B). This sequence is progressively overlapped by the Redondo Formation that is associated to extensional faulting determining progressive differential subsidence (Figure 19 C, D and E). Finally, the sedimentation of the Eocene Chira-Verdum Formation overlies the previous units establishing a homogeneous subsidence (Figure 19F).

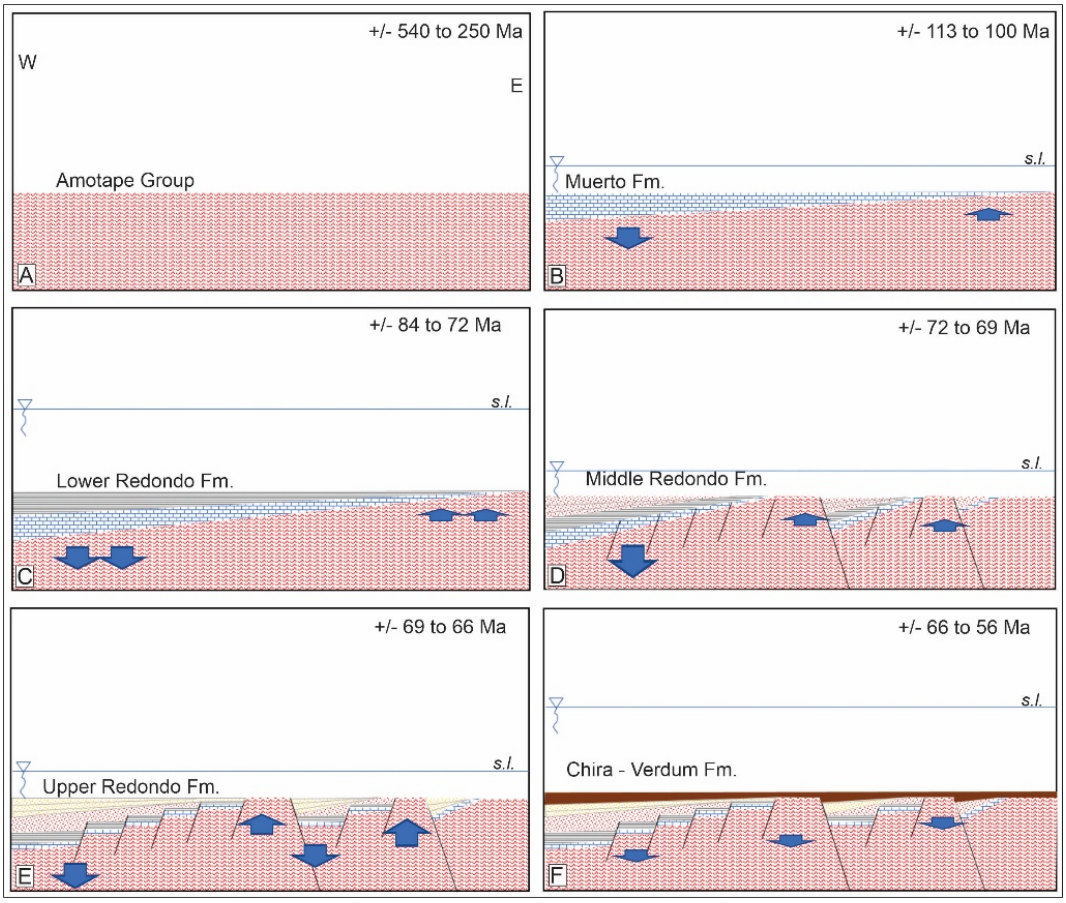

Figure 19. Evolutionary change model showing the Amotape Group faulting activity. **A**: post-Paleozoic eroded surface. **B**: Beginning of subsidence and Muerto Formation sedimentation. **C**: Subsidence increasing with the Lower Redondo Formation sedimentation. **D:** Subsidence and uplifts of Amotape Group block produced by extensional faults associated with the Middle Redondo Formation sedimentation. **E**: Increasing block movement controlling the Upper Redondo Formation sedimentation. **F**: The Chira-Verdum Formation sequence onlapping in discordance on all the sediments and exhumed Amotape Group blocks.

At least three major tectonosedimentary episodes that developed discontinuities in the Amotape Group are recognized and these determine its characteristics as an unconventional fractured reservoir:

• ***A late Palaeozoic episode*** was associated with the Carboniferous and Permo-Triassic deformation and it controlled mechanisms of diagenesis and metamorphism of the leptometamorphites of the Amotape Group. During this episode, the milky-type quartz veins were derived from segregation of protoliths made up of siliciclastic levels favoured by stylolithization. Different pulses of veins intersect, deform, and comparatively resist

the rupture of the finer leptometamorphic levels (some with carbonaceous material) that show a slate-like cleavage usually superimposed to the original sedimentary features. Granitic plutons were emplaced as stocks and dikes with syntectonic deformation.

• ***A Mesozoic episode*** was possibly associated to the Peruvian Andean (Aptian-Albian) and Inca (middle Eocene) tectonic phases, concomitant with the syntectonic deposition of siliciclastic and carbonate strata typical of the Talara Basin, that settled progressively on diachronic highs and lows of the Palaeozoic basement.

• ***A Neogene episode*** associated to the current Nazca Plate subduction mechanisms responsible of sublatitudinal state of stress and the most recent fracturing and uplift, peneplanation, and deposition of the Tablazo Formation.

DISCUSSION

Tectonic style of the Talara basin

The mentioned previous works agree that the Talara Basin is a forearc depocenter located above an active margin (Figure 4) since at least the early Mesozoic (Shepherd & Moberly, 1981; Seranne, 1987; Mourier et al., 1988; Diniz et al., 2010; Espurt et al., 2018; Lemgruber-Traby et al., 2020).

Raez (1999) defined the Talara Basin as a pull-apart basin. Grosso et al. (2005), considered it as a basin affected by various structural styles over time involving extensional, compressional and transcurrent scenarios. Oviedo & Carlotto (2013) demonstrated the importance of several compressive events in the evolution of the Talara basin recorded during the middle Eocene–early Oligocene, evidenced by the presence of folded strata, reverse faults, and thrusts associated to sedimentary and tectonic breccias.

Llerena et al. (2018) discarded the tectonic models that interpret the Talara Basin and the other forearc basins in Peru as purely extensional-type and established a new forearc tectonic model controlled by compressional deformation since the Eocene. The progressive and diachronic vertical deformation of blocks (*i.e.,* either by exhumation and erosion of highs or by subsidence of lows) would be the mechanism that explains the generation of depocenters.

The Talara Basin has complex characteristics associated with the subduction of high-altitude aseismic ridges (between 1.5 – 2.5 km). This tectonic context produces abrupt local uplifts of up to 8 mm/year such as in El Banco uplift caused by the subduction of the Alvarado Ridge in Peru (Zeumann & Hampel, 2016). Another tectonic effect on the Talara Basin of great importance is the impact of the Dolores-Guayaquil Megashear, which affects and reconfigures the direction and magnitude of the stress field (Nocquet & Calais, 2004; Nocquet et al., 2014). Seismic coupling studies show this change in stress direction as the product of the rearrangement caused by the displacement along the Dolores Guayaquil Megashear. This model validates the kinematic solutions of the faults in the field (Villega-Lanza et al., 2016). The NNW-SSE direction of the current maximum horizontal stress (σ_1) is also corroborated by information of induced fractures and/or breakouts in offshore wells through image records. Also, it is possible to determine different directions of the maximum horizontal stress evidenced in wells, responsible for different structural regimes of local areas that are currently dominated by uplift and/or subsidence events. However, these data are interpreted in terms of the shallow tectonic context of the basin (1 to 5 km depth) presumably dominated by a maximum horizontal stress with a preferential NNW-SSE direction (Villegas-Lanza et al., 2016).

Unconventional reservoir

A naturally fractured reservoir is a system with a pattern of discontinuities due to synsedimentary diagenetic changes and deformational structures due to metamorphism or tectonism. Naturally fractured systems have fractures of different sizes throughout the system with various orientations. Fractures could initially exhibit good dilating conditions, especially if they were joints, although later these may suffer alterations or filling with mineralizations. Also, further events could determine ductile deformation responses with development of multiepisodic folding.

The petrophysical characteristics of the Amotape Group obtained from borehole logging and sampling, complemented with field descriptions and available multiscale surface and subsurface information, confirm the presence of lithologies with interesting potential as a naturally fractured reservoir. The interbedded sandstone protoliths show the greatest potential to develop fractures due to their more competent mechanical behaviour that, once their limit of resistance to deformation has been surpassed, does so preferentially in a brittle manner. Also, the presence of granitic rocks and sectors with swarms of quartz veins have important potential due to

their greater probability of developing fractures and preferentially brittle behaviour.

The deepest Well 5237 penetrated 2,008 m into the Amotape Group without encountering different or older strata. Palacios (1994) described the Paita metamorphic series outcropping in the homonymous locality, attributing ages between the Ordovician – Silurian, and composed by dark grey folded micaceous pelitic slates, schists and quartzites, showing intraformational faulting. There are also sandstones and schistose, greenish grey shales with thin bedding. The sequence generally strikes 20° E and 40° E, dipping between 40° and 60° to the northeast. Based on petrophysical, petrographic, and electronic microscopy, some sections particularly quartzite exhibit porosity value ranging between 4.62 and 1.23% and permeabilities of 0.519 to 0.016 mD. The elevated topographic position of the Amotape Group in the Talara basin offers a very good chance for trapping hydrocarbons when these appear conveniently sealed by Cretaceous sequences. The exposure the Amotape Group before Cretaceous deposition through uplift and consequent erosive processes, allowed the development of increased fracturing associated to discrete edaphic phenomena. This subaereal process contributed to provide unconventional reservoir characteristics to the upper portions of the Amotape Group.

The hydrocarbon production in Amotape Group is associated primarily to highly fractured quartzite facies, although there are also some metaargillite zones competent enough to support open fractures that can store and yield oil. Pozo-Calle & Castillo-Guzmán (2018) mentioned initial production rates varying between 20 and 1025 BOPD (Figure 20A). Prado-Paucar (2018) contended that some secondary porosity is related to natural fractures, especially in positions near to post-Amotape Group unconformity and to large-leap faulting where total porosity in quartzite (combining both fracture and intergranular porosity) is reported averaging 5%. Intergranular porosity measured in borehole cuts ranges between 0.7 and 5% and the average permeability is indicated as 4 mD).

These petrological and petrophysical characteristics of the Amotape Group open the possibility of supposing hydrocarbon production. Baseline studies also revealed some secondary porosity related to natural fractures (Figure 20B**)**, especially near the post-Amotape unconformity and in the vicinity of faulting that bounds differentially uplifted or dropped blocks. Diniz et al. (2010) recognized from the analysis of 25 fault planes in the 3D seismic in the area the following main directions in the Amotape Group: N20E, N65W, N20W and N85E.

Nelson (2001) proposed a classification for naturally fractured reservoirs based on the positive effect of fractures on reservoir transport properties (Figure 20C):

- Type 1 – Fractures provide the essential porosity (*i.e.*, storage capacity) and flow capacity in a reservoir where matrix porosity and permeability are low. In this type of reservoir, fracture characteristics are the dominant parameters for reservoir evaluation and few producing wells are required to deplete the reservoir.
- Type 2 – Rock matrix has higher porosity whereas fractures provide the essential flow capacity in a reservoir. In this case, crossflow between fractures and matrix and rate control are key parameters, with hydrocarbon production being dominated by fractures (Type G).
- Type 3 – The fractured reservoir is already economically producible (high porosity and permeability in the matrix), and the fractures provide a support and tend to define anisotropy properties of reservoir's flow.
- Type 4 – Fractures, which could be partially filled with cementing agents acting as baffles and barriers to flow in an already producible reservoir and reducing the drainage and sweep efficiency.
- Type M - Fractures provide no additional porosity or permeability but create significant reservoir anisotropy (barriers).

Faulting related to an unconventional reservoir

Fracture networks provide flow paths at different scales, and permeability enhancement under these conditions depends on factors such as fracture intensity and density, spatial orientation, and hydraulic conductivity of the different fracture planes. This causes fluid within the matrix continuum to flow into the fracture continuum, where it is removed through the wells connecting to the fracture continuum. Mechanical behaviour of fractured rocks is complex and usually influenced by a variety of factors including spatial relationship between stress field and fractures, rock elastic properties, interface friction, surface adhesion, surface roughness, and presence of fluids and debris at interfaces.

To fully characterize naturally fractured reservoirs, it is necessary to determine the fracture-

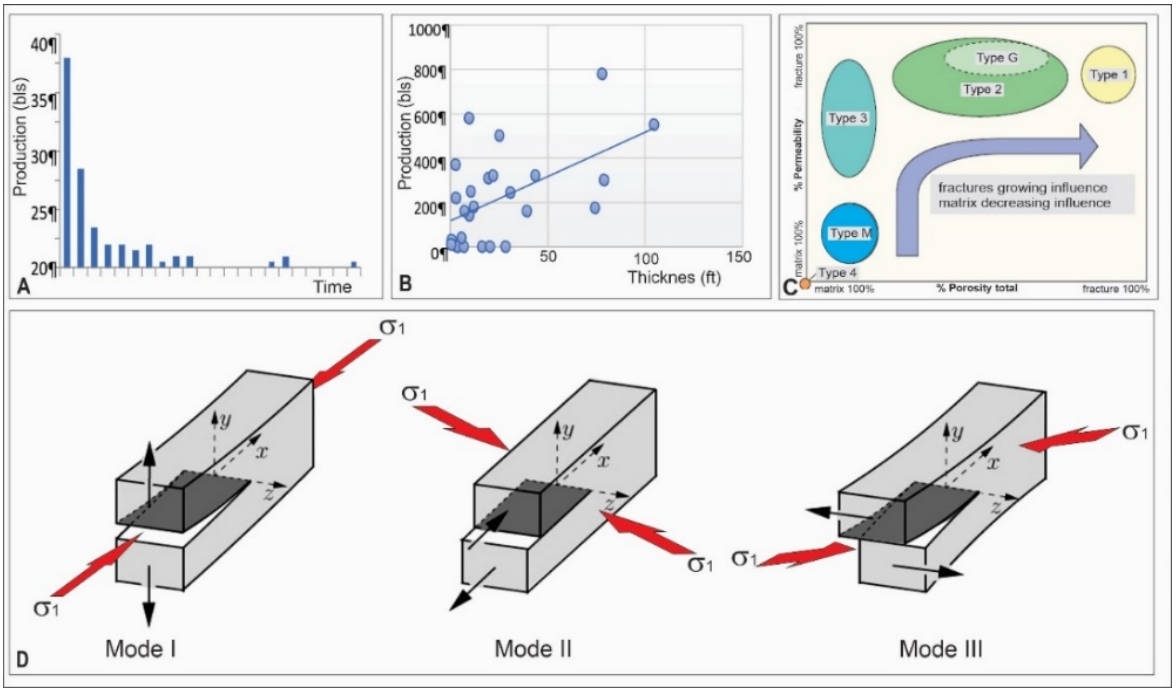

Figure 20. A: Amotape Group production *vs*. daily average (taken from Pozo-Calle & Castillo-Guzmán, 2018). **B:** Quarzitic thickness (ft) *vs.* oil production (BPPD). **C:** Types of reservoirs based on porosity and permeability (taken from Nelson, 2001). **D**: Three different crack opening types (taken from Gross & Seelig, 2006).

matrix system and to know the magnitude and orientation of the principal stresses, which are obtained through geomechanical methodologies. Based on the stress field, Nelson (2001) described three different types of fracture behaviour: i) Mode I describes a symmetric joint fracture opening (with respect to x-z plane) under a normal tensile stress, ii) Mode II corresponds to fracture slip (in x-direction normal to the fracture front) under in-plane (co-directional) shear stress, and iii) Mode III denotes the fracture tearing (in z-direction tangential to fracture front) as a result of out-of-plane shear stress (Figure 20D).

Barenblatt et al. (1960) considered dual-porosity models consisting of two contiguous (superposed) continuums, those being matrix-blocks (primary pores) and fractures (secondary pores), which configure a gradient on its own fluid pressure system, *i.e.*, between the fluid in the matrix pores and the adjacent fractures, that is maintained during production. Nelson (2001) classified naturally fractured reservoirs based on the ratio of porosity versus system permeability (Figure 20C). According to this classification, the Amotape Group case is closer to a type 2: since the matrix has low porosity and low permeability, it operates as a complementary reservoir for hydrocarbons where fractures provide a large part of the permeability system. However, the matrix also contributes to it, as it is corroborated by the typical production curve of the reservoir.

Jalali & Dusseault (2012) asserted that geomechanics has increasingly become part of oil industry analysis, based on their approaches to explain and evaluate phenomena such as wellbore stability in shale, reservoir compaction and surface subsidence during depletion, sand production during well drawdown, and hydraulic fracture stimulation. The behaviour of pressure tests, where there are observed, shows that the permeability of the system reaches 3 to 20 times more than that interpreted by logs, outcrop evidence, aerial images, cores and well image logs. Rossello et al. (2002, 2005) described examples of the equivalent unconventional reservoirs currently being exploited in granitic and volcanic rocks that underlie the traditional reservoir levels of the Neuquén Basin. Also, ophiolite sequences in the northern belt of Cuba have been producing hydrocarbons for decades (Rossello & García-Sánchez, 2017). The Amotape Group lithologies, originally considered technical basement without porosity and primary permeability, could provide good reservoir conditions if those are affected by fractures. In general, these secondary characteristics are a combined result of the generation of tectonic microfractures and differential alterations of mineral constituents.

This compressional context favors the development of fractures in the Amotape Group, where the preferential direction of the last responsible stress field can be located. The knowledge of the spatial position of the stress field conditionates the design of the most effective orientation of the

productive drillings where the preferential direction of production wells must coincide with that of the minimum principal stress (σ_3) (Rossello, 2018; López-Gamundí & Rossello, 2021).

The majority of the potentially open fractures in the Amotape Group observed in outcrop and interpreted in the seismic survey of the Colan Block as subparallel to normal faulting tend to be subvertical with sub latitudinal to ENE-WSW strikes. With respect to this fracture pattern, the ideal orientation for future exploration and production wells should be NNW-SSE in plan, as this is the orientation of minimum principal stress (σ_3) (Figure 21).

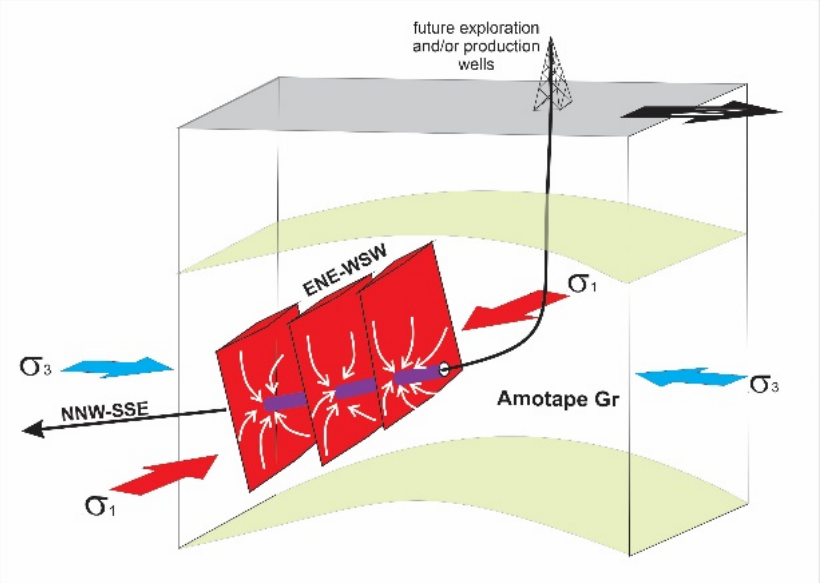

Figure 21. Schema of the best orientation of a well-directed subparallel to σ_3 (NNW-SSE) in order to cross the major number of potentially open fractures (joints) per linear meter (modified from Rossello, 2018).

CONCLUDING REMARKS

The definition of a non-traditional exploratory objective was addressed from the multidimensional perspective of a petroleum system associated with an unconventional reservoir. Based on integrated multiscale surface and subsurface data, the Paleozoic Amotape Group exhibits in the surroundings of the Colán Block, close to Paita city multi-reservoir strata predominantly of quartzite facies, which, due to its structural position, composition, texture and structures, and Cretaceous rock cover, constitute key variables for hydrocarbon production success. The Colán X139 well, shows up to seven bodies of quartzite sandstones with thicknesses ranging between 100 and 400 feet and thinning towards the North. The porosity values of the Amotape Group range between 4.62% and 1.23%, while permeabilities are on the order of 0.519-0.016 mD.

Petrographic data obtained from lateral samples in well Colán X139 support the subdivision of Amotape Group into three main lithological types, separated by 200- and 476-ft respectively. The shallower lithological unit (1,915 and 1,917 ft) corresponds to carbonate rocks, the second unit (2,117 and 2,121 ft) to medium to fine metasandstones, and the third dominant unit (2,597 to 3,215 ft) to cataclastic quarzitic sandstones. The lithological logs and core descriptions indicate that the highest percentage of Amotape rocks consists of metamorphic rocks from sedimentary quartzitic sandstones and argillite facies. The most important visual secondary porosity (microfracture) is shown with greater density and opening in the quartzite facies, which increase up to 5% the effective porosity. The whole porosity combined with intergranular and fracture porosity in the quarzitic core is reported to be averaging 5%, ranging between 0.7 and 5%. The average permeability is indicated as 4 mD, but the initial production ratio in the Colán X139 well varies between 20 to1,025 BOPD, which makes this value incongruous without considering the contribution of the fractures.

Three tectonosedimentary episodes are recognized: i) ***a late Palaeozoic episode*** of diagenesis and metamorphism defined by slate-like cleavage intruded by pulses of quartz veining, associated to Carboniferous and Permian-Triassic tectonic phases, (ii) ***a Mesozoic episode*** of syntectonic deposition of siliciclastic and carbonate sequences typical of the Talara Basin, exhibiting progressive settlement on diachronic highs and lows of the Palaeozoic basement possibly developed during the Peruvian Andean

(Aptian-Albian) and Inca (middle Eocene) tectonic phases, and (iii) ***a Neogene episode*** expressed as the most recent event of fracturing, uplift, erosion and peneplanation of blocks, and deposition of the Tablazo Formation, during the Andean-Quechua tectonic phase under the domain of Nazca-South America convergence.

The tectonic model of the Colan Block would have resulted from a compressive tectonic context affecting previous normal faults with regional wrench-type faults parallel to the trench (NNW-SSE) and their fault conjugates (ENE-WSW). Continuous and diachronic block uplift would have been the mechanism for the generation of depocenters (subsidence) and the erosion of structural highs. The normal faults are mainly explained by transtension or gravitational faults as a product of the uplift of blocks but not by pure extensional tectonics.

The presence of the fracture pattern in the Amotape Group constitutes an unconventional hydrocarbon target in the economic basement complementary to the traditional Cretaceous-Cenozoic petroleum systems of the basins that overlie it. In the case of perforating exploration and production wells in these rocks, should be drilled following the direction of the minor compressive stress of the last tectonic episode along the NW-SE trend, since this orientation will have the greatest chance of crossing the bigger number of potentially dilating fractures per linear meter.

ACKNOWLEDGMENTS

We thank the company Olympic Zeuss Energy for facilitating access to subsurface information and also to colleagues who enriched the content of this work with comments and fruitful discussions. In addition, we are grateful for the many and timely comments received during the editorial treatment that improved the understanding of the work. The authors declare that they have no known competing financial interests or personal relationships that could have appeared to influence the work reported in this paper.

REFERENCES

AIZPRUA, C., WITT, C., JOHANSEN, S.E., BARBA, D. Cenozoic stages of forearc evolution following the accretion of a sliver from the Late Cretaceous-Caribbean Large Igneous Province (CLIP): SW Ecuador-NW Peru. Tectonics 38 (4): 1441-1465. 2019. https://doi.org/10.1029/2018TC005235

ARISPE, A. Peru offshore 1: Peru offers deep-water blocks south of Talara area. *Oil & Gas Journal*, 99 (8): 25-29. 2001a.

ARISPE, A. Peru offshore 2: Tumbes -Talara blocks off Peru may signal deep-water play in turbidites. *Oil & Gas Journal*, 99 (7): 21-24. 2001b.

BARENBLATT, G., ZEHLTOV, I., KOCHINA, I. Basic concepts in the theory of seepage of homogeneous liquids in fissured rocks. Journal of Applied Mathematics and Mechanics, 24: 1286-1303. 1960.

BELLIDO, F., JAIMES, F., CARLOTTO, V., DÍAZ MARTÍNEZ, E. Los granitoides peralumínicos triásicos de los Cerros de Amotape y del Macizo de Illescas (Noroeste de Perú): Implicaciones para la evolución geodinámica del Terreno Amotape. XIV Congreso Peruano de Geología y XIII Congreso Latinoamericano de Geología, Lima, Perú, CD-ROM, G-07, 6 p. 2008.

BELLIDO, F., VALVERDE, P., JAIMES, F., CARLOTTO, V., DÍAZ-MARTÍNEZ, E. Datación y caracterización geoquímica de los granitoides peralumínicos de los Cerros de Amotape y de Los Macizos de Illescas y Paita (Noroeste de Perú). Bol. Soc. Geol. Perú 103: 197-213. 2009.

BIANCHI, C. & JACAY, J. Evolución paleogeográfica fanerozoica de la región nor-occidental de la margen peruana y sus posibilidades hidrocarburíferas. Boletín de la Sociedad Geológica del Perú, 110: 110-114. 2015.

BOSWORTH, T.O. Geology of the Tertiary and Quaternary periods in the NW – Peru. Geological Magazine, 60 (1): 43 – 45. 1923.

BOURGOIS, J., BIGOT-CORMIER, F., BOURLES, D., BRAUCHER, R., DAUTEUIL, O., WITT, C., MICHAUD, F. Tectonic record of strain buildup and abrupt coseismic stress release across the northwestern Perú coastal plain, shelf, and continental slope during the past 200 kyr. Journal of Geophysical Research, 112: B04104, 2007. doi: 10.1029/2006JB004491.

CALDAS, J. Complejo metamorfico de Illescas. Boletín de la Sociedad Geológica del Perú, 63: 217-235. 1979.

CARDONA, A., CORDANI, U.G., RUIZ, J., VALENCIA, V.A., ARMSTRONG, R., CHEW, D., NUTMAN, A., SÁNCHEZ, A.W. U-Pb zircon geochronology and Nd isotopic signatures of the pre-Mesozoic metamorphic basement of the eastern Peruvian Andes: growth and provenance of a late Neoproterozoic to Carboniferous accretionary orogen on the northwest margin of Gondwana. Journal of Geology, 117: 285–305. 2009.

CAROZZI, A.V. & PALOMINO, J.R. The Talara forearc basin, NW Peru: Depositional models of oil-producing Cenozoic clastic systems. Journal of Petroleum Geology 16 (1): 5–32. 1993.

CHLIEH, M., Distribution of discrete seismic asperities and aseismic slip along the Ecuadorian megathrust. Earth and Planetary Science Letters 400: 292-301 pp. 2014.

CHLIEH, M., PERFETTINI, H., TAVERA, H., AVOUAC, J.-P., REMY, D., NOCQUET, J.-M., ROLANDONE, F., BONDOUX, F., GABALDA, G., BONVALOT, S. Interseismic coupling and seismic potential along the Central Andes subduction zone. J. Geophys. Res. Solid Earth, 116(B12405), 1-21, 2011. doi:10.1029/2010JB008166.

CHOQUETTE, P.W. & PRAY, L.C. Geologic Nomenclature and Classification of Porosity in Sedimentary Carbonates. American Association of Petroleum Geologists, Bulletin, 54, 207-250. 1970.

COBBOLD, P.R., ROSSELLO, E.A., ROPERCH, P., ARRIAGADA, C., GÓMEZ, L.A., LIMA, C. Distribution, timing, and causes of Andean deformation across South America. In: Ries, A.C., Butler, R.W.H., Graham, R.H. (eds.), Deformation of the continental crust: The legacy of Mike Coward. Geological Society of London, Special Publications 272: 321-343, 2007. London.

DAUDT, J. & SCHERER, C.M. Arquitetura de fácies e evolução estratigráfica dos reservatórios flúvio-deltaicos da Formação Echinocyamus (Eoceno Inferior) na área do Lote 10 (Bacia de Talara, Noroeste do Peru). Boletim de Geociências da Petrobras 14 (1), 27-45. 2006.

DAUDT, J., POZO, G., TORRES, K., ORE, L. Evolução estratigráfica, arcabouço estrutural e potencial remanescente das unidades produtoras da Bacia de Talara (noroeste do Peru) na área do Lote X. Boletim de Geociências da Petrobras 18: 69-95. 2010.

DE VRIES, T.J. The geology of late Cenozoic marine terraces (Tablazos) in northwestern Peru. Journal of South American Earth Sciences 1: 121-136. 1988.

DICKINSON, W.R. Forearc basins. In: Busby, C.J., Ingersoll, R.V. (eds.), Tectonics of sedimentary basins, Blackwell Science, 221-261, 1995. Oxford.

DINIZ, S.H., DE SÁ, F.R., RODRÍGUEZ, C., SANTOS, C.G., CRUZ, J.M.N., BEAS, W.E. Talara Basin, Peru: Structural and Stratigraphic Characterization Based on 3D-Seismic Data. Society of Petroleum Engineers, SPE 139283, 8p. 2010.

DUNHAM, R.J. Classification of carbonate rocks according to depositional texture. In: Ham, W.E. (ed.), Classification of Carbonate Rocks. American Association of Petroleum Geologists, 108-121, Tulsa. 1962.

FOLK, R.L. Petrology of sedimentary rocks. Hemphill Publishing Co., 170 p., 1974. Austin.

ESPURT, N., BRUSSET, S., BABY, P., HENRY, P., VEGA, M., CALDERON, Y., RAMÍREZ, L., SAILLARD, M. Deciphering the Late Cretaceous-Cenozoic structural evolution of the North Peruvian forearc system. Tectonics 37: 251-282. 2018. doi.org/10.1002/2017TC004536

FILDANI, A., HANSON, A.D., CHEN, Z., MOLDOWAN, J.M., GRAHAM, S.A., ARRIOLA, P.R. Geochemical characteristics of oil and source rocks and implications for petroleum systems, Talara basin, northwest Peru. AAPG Bulletin, 89 (11): 1519-1545. 2005.

FILDANI, A., HESSLER, A.M., GRAHAM, S.A. Trench-forearc interactions reflected in the sedimentary fill of Talara basin, northwest Peru: The Talara Forearc basin. Basin Research, 20 (3): 305–331. 2008.

GONZALES, E. & ALARCÓN, P. Potencial hidrocarburífero de la cuenca Talara. Lima, Peru. *INGEPET 2002* Seminar, EXPR-1-EG-07, 15 pp. 2002.

GROSS, J. & SEELIG, T. Fracture Mechanics with an Introduction to Micromechanics. Springer 326 pp. 2006. The Netherlands.

GROSSO, S., MARCHAL, D., DAUDT, J. Integración afloramiento-subsuelo: relación entre la complejidad estructural y el comportamiento productivo de los reservorios del Lote X, cuenca Talara, Perú. V Seminario Internacional de Exploración y Producción de Petróleo y Gas – INGEPET, Lima-Perú. 2005.

HIGLEY, D. The Talara basin province of northwestern Peru. Cretaceous-Tertiary total petroleum system. U.S. Geological Survey, e-bulletin B-2206a: 52 p. 2004. http://pubs.usgs.gov/bul /2206/A/.

HINOSTROZA, C. & ESPINOZA, U. Incremento de producción mediante la rehabilitación y seguimiento de pozos abandonados en campos maduros: un ejemplo - Lote X, Talara – Perú. V° INGEPET (EXPL-4-CH-150), 12p. 2005.

IDDINGS, A. & OLSSON, A.A. Geology of Northwest Peru. American Association of Petroleum Geologists, Bulletin 12:1-39. 1928.

JALALI M.R. & DUSSEAULT, M.B. Coupling geomechanics and transport in Naturally Fractured Reservoirs. International Journal Mining & Geo-Eng., 46 (2): 105-131. 2012.

JAILLARD, E. Evolución de la margen andina en el norte del Perú desde el Aptiano superior hasta el Senoniano. Bol. Soc. Geol. Perú, 81, 3-13. 1990.

JAILLARD, E., LAUBACHER, G., BENGTSON, P., DHONDT, A., PHILIP, J., BULOT, L., ROBERT, E. Revisión estratigráfica del Cretáceo Superior del noroeste peruano y suroeste ecuatoriano. Datos preliminares, consecuencias tectónicas. Boletín de la Sociedad Geológica del Perú, 88: 101-115. 1998.

JAILLARD, E., HÉRAIL, G., MONFRET, T., DÍAZ-MARTÍNEZ, E., BABY, P., LAVENU, A., DUMONT, J.F. Tectonic evolution of the Andes of Ecuador, Perú, Bolivia and northernmost Chile. In: Cordani, U.G., Milani, E.J., Thomaz Filho, A., Campos, D.A. (eds.). Tectonic Evolution of South America. 31st International Geological Congress, Rio de Janeiro 481-559. 2000.

KELLEHER, J.A. Rupture Zones of Large South American Earthquakes and Some Predictions. Journal Geophysical Research, *77*(11): 2087-2103. 1972.

LAL, D. The present scope of the field of terrestrial cosmogenic nuclides, Science, 6, 744–751. 1991a.

LAL, D. Cosmic ray labelling of erosion surfaces: In situ nuclide production rates and erosion models, Earth Planet. Sci. Lett., 104, 424–439. 1991b.

LCV. Oly-Colán-XIII-5-139X and PN wells. Sidewall cores and cuttings Redondo, Muerto and Amotape Formations. Lithologic, petrographic, diagenetic, mineralogic, scanning electron, microscope and petrophysical study. Olympic Perú Inc., Sucursal del Perú. Internal Report, 25pp. 2019.

LEMGRUBER-TRABY, A., ESPURT, N., SOUQUE, C., HENRY, P., CALDERON, Y., BABY, P., BRUSSET, S. Thermal structure and source rock maturity of the North Peruvian forearc system: Insights from a subduction-sedimentation integrated petroleum system modeling. Marine and Petroleum Geology 122, 104664. 2020. 10.1016/ j.marpetgeo. 2020.104664.

LLERENA, C.E., ROMERO, D., BENIQUE, A., LEE, K. Análisis estructural de la Cuenca Talara - Resultados preliminares. IX INGEPET 2018 (GEO-EX-CL-17-N). 18 pp. 2018.

LÓPEZ-GAMUNDÍ, O.R., ROSSELLO, E.A. The Permian Tunas Formation (Claromecó Basin, Argentina): Potential naturally fractured reservoir and/or coal bed methane (CBM) play?. Marine and Petroleum Geology. 128: 104998. 2021.

MAGOON, L.B.; DOW, W.G. The petroleum system. *In*: Magoon, L.B.; Dow, W.G. (Eds.), The petroleum system-From source to trap. *American Association of Petroleum Geologists, Memoir* 60: 3-23. 1994.

MARTÍNEZ, M. Geología del Basamento Paleozoico en la Montañas de Amotape y posible origen del petróleo en rocas Paleozoico del NO del Perú. Primer Congreso Latinoamericano de Geología. 1970.

MARSAGLIA, K.M. & CAROZZI, A.V. Depositional environment, sand provenance, and diagenesis of the basal Salina Formation (lower Eocene), NW Peru. Journal South American Earth Sciences 3: 253-267. 1991.

MOURIER, T., L.A.J., C., MÉGARD, F., ROPERCH, P., MITOUARD, P., FARFÁN MEDRANO, A. An accreted continental terrane in northwestern Peru. Earth and Planetary Science Letters, 88: 182-192. 1988.

MURANY, E. Tectonic framework of Northwest Peru. Exploration Report 75-09. Belco Perú. 1975. NOAA, National Oceanic and Atmospheric Administration. http://www.noaa.gov/

NAUSS, W. A Reconnaissance Geological Survey of the La Brea Mountain Front. Reporte Interno Petroperú. Nº 121-2. 1944.

NELSON, R.A. Geologic analysis of naturally fractured reservoirs. Gulf Professional Publishing (2nd ed.). 2001.

NEWELL, N.D., CHRONIC, J., ROBERTS, T.G. Upper Paleozoic of Peru. Geology of South America, The Geological Society of America, Memoir 58, 276 pp. 1949.

NOCQUET, J.M. & CALAIS, E. Geodetic measurements of crustal deformation in the Western Mediterranean and Europe. Pure Appl. Geophys., 161(3): 661-681, 2004. doi:10.1007/s 00024-003-2468-z.

NOCQUET, J.M., VILLEGAS, J.C., CHLIEH, M., MOTHES, P.A., ROLANDONE, F., JARRIN, P., CISNEROS, D., ALVARADO, A., AUDIN, L., BONDOUX, F., MARTIN, X., FONT, Y., RÉGNIER, M., VALLÉE, M., TRAN, T., BEAUVAL, C., MAGUIÑA MENDOZA, J.M., MARTÍNEZ, W., TAVERA, H., YEPES, H. Motion of continental slivers and creeping subduction in the northern Andes. Nature Geoscience, 7 (8): 612. 2014.

NORABUENA, E., LEFFLER-GRIFFIN, L., MAO, A.,

DIXON, T., STEIN, S., SACKS, I.S., OCOLA, L., ELLIS, M. Space geodetic observations of Nazca-South America convergence across the Central Andes, Science (80) 279 (5349): 358–362, 1998. doi:10.1126/science.279.5349.358.

OVIEDO, M. & CARLOTTO, V. Repeticiones estratigráficas y brechas asociadas a un evento compresivo Eoceno medio–superior en la cuenca Talara, sector El Alto-Cabo Blanco-Peña Negra, Piura, Perú. Boletín de la Sociedad Geológica del Perú, 108: 144-147. 2013.

PALACIOS, O. Geología de los cuadrángulos de Paita, Piura, Talara, Sullana, Lobitos, Quebrada Seca, Zorritos, Tumbes y Zarumilla. Boletín Nº 54. Serie A. Carta Geológica Nacional. INGEMMET, Perú, 19pp. 1994.

PALACIOS, M.O., SÁNCHEZ, Y.J., SHAW, R., PILATASIG, L., GORDON, D. Entidad Paleozoica en la Faja Amotape-Tahuin y Cordilleras Occidental (Perú) y Real (Ecuador). 12° Congreso Peruano de Geología. Resúmenes Extendidos. 2004.

PEDOJA, K., ORTLIEB, L., DUMONT, J.F., LAMOTHE, M., GHALEB, B., AUCLAIR, M., LABORUSSE, B. Quaternary coastal uplift along the Talara Arc (Ecuador, Northern Peru) from new marine terrace data. Marine Geology 228: 73-91. 2006.

PRADO-PAUCAR, A. Integración de datos geológicos y geofísicos en el modelo del Intra-Amotape, Yacimiento Portachuelo – Lote III. IX INGEPET 2018 (GEO-DE-AP-12-N), 15 pp. 2018.

PERUPETRO, S.A. Estudio geológico del basamento Paleozoico en las montañas Amotape. Perupetro S.A. Technical Archive IT 00255. 1970.

PERUPETRO Statistics. 2020.. https://www.perupetro.com.pe/wps/portal/corporativo/PerupetroSite (February 20th 2022)

PINDELL, J.L., TABBOT, K.D. Mesozoic - Cenozoic Andean paleogeography and regional controls on hydrocarbon systems. *In:* Tankard, A.J.; Suárez Soruco, R.; Welsink, H.J. (eds.), Petroleum basins of South America. American Association of Petroleum Geologists, Memoir, 62: 101 – 128. 1995.

PORTELLA VILLACHICA, G. Potencial de gas no asociado en la Formation. Salina Mogollón. Zona C- Lote III. Cuenca Talara. IX INGEPET 2018 (GEO-DE-GP-07-N). 21 pp. 2018.

POZO-CALLE, G. & CASTILLO-GUZMÁN, E. Recursos no convencionales: Estimación preliminar Sistema Petrolero Muerto, Cuenca Talara -PERÚ IX INGEPET 2018 (GEO-EX-GP-07-N). 14pp. 2018.

RAEZ, M.A. Tectónica en la cuenca Talara costa-afuera, Nor Oeste del Perú. INGEPET '99, Lima, EXPR-1-MR-12. 1999.

ROSSELLO, E.A. Interpretaciones estructurales dinámicas a partir del análisis de ovalización (break-outs) de pozos: aplicaciones a perforaciones en la Formación Vaca Muerta (Cuenca Neuquina, Argentina). Revista de la Asociación Geológica Argentina, 75 (2): 252-264. 2018.

ROSSELLO, E.A. & BARRIONUEVO, M. El hemigraben invertido del yacimiento 25 de Mayo - Medanito SE (Cuenca Neuquina, Argentina): evolución geodinámica de un rift en borde de cuenca. VI° Congreso de Exploración y Desarrollo de Hidrocarburos, Simposio Trampas (Mar del Plata). Memorias CD-Rom. 2005.

ROSSELLO, E.A. & GARCÍA-SÁNCHEZ, R. Trampas no convencionales asociadas a ofiolitas de la Faja Septentrional de Hidrocarburos (La Habana-Matanzas, Cuba). Boletín de Geología (UIS, Bucaramanga, Colombia) 39 (3): 41-54. ISSN: 0120-0283 (PRINT) ISSN: 2145-8553 (WEB). 2017. DOI: http://dx.doi.org/10.18273/revbol.

ROSSELLO, E.A., COSSEY, S., FERNÁNDEZ, G. The offshore hydrocarbon origin of the Talara field (Perú). Andean Geology 49 (1)*:* 10.5027/andgeoV49, n1-3383. 2022.

ROSSELLO, E.A., COBBOLD, P.R., DIRAISON, M., ARNAUD, N. Auca Mahuida (Neuquén Basin, Argentina): A Quaternary shield volcano on a hydrocarbon-producing substrate. 5th International Symposium on Andean Geodynamics (Toulouse). 549-552. 2002.

SCHMIDT, V.M. & McDONALD, D.A. The role of secondary porosity in the course of sandstone diagenesis. In: SCHOULE, P.A. & SCHLUGER, P.R. (eds.). Aspects of diagenesis. SEPM Special Publication 26: 175 – 207. 1979. doi.org/10.2110/pec. 79.26. 0175

SERANNE, M. Evolution tectono-sedimentaire du Bassin de Talara (nord-ouest du Perou). Bulletin de l'Institut Français des Études Andines 16 (3-4): 103-125. 1987.

SHEPHERD, G.L. & MOBERLY, R. Coastal structure of the continental margin, northwest Peru and southwest Ecuador. Geological Society of America, Memoir 154: 351-391. 1981.

SILGADO, E. Historia de los sismos más notables ocurridos en el Perú (1513-1974), 1978. Lima.

SPIKINGS, R.A., WINKLERB, W., HUGHESC, R.A., HANDLER, R. Thermochronology of allochthonous terranes in Ecuador: Unravelling the accretionary and post-accretionary history of the Northern Andes. Tectonophysics 399: 195-220. 2005.

STERN, R.J. Subduction zones. Review of Geophysics. 40, Issue 4. 2002. https://doi.org/10.1029/ 2001rg000108

TRAVIS, R.B., GONZALES, G., PARDO, A. Hydrocarbon potential of coastal basins of Peru. American Association of Petroleum Geologists, Special Volumes, M 25: Circum-Pacific Energy and Mineral Resources, 331-338. 1976.

VILLEGAS-LANZA, J.C., CHLIEH, M., CAVALIÉ, O., TAVERA, H., BABY, P., CHIRE-CHIRA, J., NOCQUET, J.M. Active tectonics of Perú: Heterogeneous interseismic coupling along the Nazca megathrust, rigid motion of the Peruvian Sliver, and Subandean shortening accommodation. Journal of Geophysical Research: Solid Earth. Research article 2016. 10.1002/2016JB013080.

VALENCIA, K., LLERENA, C. El play exploratorio paleozoico de la Cuenca Talara, el futuro económico de la cuenca. IX INGEPET 2018 (GEO-EX-KV-24-N). pp. 27. 2018.

WIPF, M. Evolution of the Western Cordillera and Coastal Margin of Peru: Evidence from low temperature Thermochronology and Geomorphology. 2006. Swiss Fed. Inst. of Tech. Zurich. PhD Thesis.

WITT, C., BOURGOIS, J. Forearc basin formation in the tectonic wake of a collision-driven, coastwise migrating crustal block: The Example of the North Andean Block and the extensional Gulf of Guayaquil-Tumbes Basin (Ecuador-Peru Border Area); Geological Society of America Bulletin, 122 (1-2): 89-108. 2010.

ZEUMANN, S. & HAMPEL, A. Three-dimensional finite-element models on the deformation of forearcs caused by aseismic ridge subduction: The role of ridge shape, friction coefficient of the plate interface and mechanical properties of the forearc. Tectonophysics. 2016. TECTO-126888

ZÚÑIGA-RIVERO, F., HAY-ROE, H., VARGAS, T. Talara: A new look at an old petroleum basin. Exploration and exploitation of petroleum and gas: Lima, Peru. INGEPET '99, EXPR-1-FZ-15, 9 p. 1999a.

ZÚÑIGA-RIVERO, F., HAY-ROE, H., VARGAS, T. Peru's coastal basin-5 (conclusion), Potential untested under 50 million acres in Peru. Oil & Gas Journal 97 (11): 67-72. 1999b.

Submetido em 17 de março de 2024
Aceito para publicação em 7 de junho de 2024